1 **The Early – Middle Pleistocene Transition in the Gulf of Cadiz (NE Atlantic) – an**

2 **interplay between subtropical gyre and extremely cold surface waters**

4 Aline Mega[1,2] (0000-0002-9386-2261), Teresa Rodrigues[1,2] (0000-0001-7811-7506), Emília

5 Salgueiro[1,2] (0000-0003-1000-2977), Mária Padilha[1] (0000-0002-7103-5695), Henning

6 Kuhnert[3] (0000-0001-5242-4495), Antje H. L. Voelker[1,2] (0000-0001-6465-6023)

8 [1]Divisão de Geologia e Georecursos Marinhos, Instituto Português do Mar e da Atmosfera

9 (IPMA), Avenida Doutor Alfredo Magalhães Ramalho 6, 1495-165 Alges, Portugal.

10 [2]Centro de Ciências do Mar, University of the Algarve, Campus de Gambelas, 8005-139 Faro,

11 Portugal.

12 [3]MARUM, Universität Bremen, Leobener Straße 8, 28359 Bremen, Germany.

13 *Correspondence to*: Aline Mega (alinemega20@gmail.com)

15 **Abstract.** Besides the shift in dominant orbital cyclicity depicted in paleoclimate proxy

16 records, the mid-Pleistocene Transition or Early-Middle Pleistocene Transition (EMPT) was

17 linked to a change in the deep thermohaline circulation. Those changes contributed to more

18 intense and longer-lasting glacial periods and cooler sea surface temperatures (SSTs) during

19 glacials. Within the Atlantic Ocean, the Iberian margin is considered a key location to study

20 climatic variations influenced by both high- and low-latitude processes. In this study we focus

21 on IODP Site U1387 on the southern Portuguese margin to reconstruct surface water circulation

22 changes and related plankton foraminifera ecosystems during the interval of Marine Isotope

23 Stage (MIS) 28 to MIS 18 (1006-750 ka). Our planktonic foraminifera assemblages and SST

24 reconstructions (foraminifera assemblages and $U^{K'}_{37}$ alkenone index) demonstrate warm,

25 relative stable SST conditions during much of the interval due to persistent influence of

26 subtropical gyre waters as indicated by the tropical-subtropical and Azores Current related

27 foraminifera species and the periods with dominant sinistral coiling direction of the species

28 *Globorotalia truncatulinoides*. Maximum interglacial SSTs were up to 2ºC warmer than at

29 present in both summer and winter, with the exception of interglacial MIS 23 with SSTs ~1.5°C

30 colder than in the other interglacials. Subsequent the respective glacial inception, the relative

31 warm conditions were periodically interrupted by millennial-scale extreme cold events when

32 polar species *Neogloboquadrina pachyderma* became abundant (>30%) and the SSTs,

reconstructed from the foraminifera assemblage data, dropped below 10°C in summer and 5 °C in winter, although some of those values might be overestimated. The most pronounced event, considering the amplitude of cooling and duration, occurred between 870 to 864 ka, marking the terminal stadial event of the MIS 22/MIS 21 transition (Termination X). Extreme cold events, always associated with the incursion of subpolar waters into the Gulf of Cadiz, mark all the terminal stadial events from Terminations XII to IX and the millennial-scale variability during the transitions to full glacial conditions, although the duration of the cooling varied greatly. The extreme cooling was only possible through migration of the subarctic front into the lower mid-latitudes as a consequence of cooling and freshening in the higher latitudes and the associated extreme reduction in the Atlantic meridional overturning circulation. The amplitude of cooling, duration, and frequency of subpolar water incursions during MIS 24 to MIS 22 stands out, providing further evidence for the "900 ka event" being a key feature of the EMPT.

1. Introduction

A major global climatic shift, known as the mid-Pleistocene or Early-Middle Pleistocene Transition (EMPT), took place between 1250 and 650 thousand years (ka) ago, dramatically changing Earth's climate dynamics (Clark, 2012; Clark et al., 2006; Head and Gibbard, 2015; McClymont et al., 2013). This period was characterized by long-term cooling in global mean sea surface temperatures (SSTs), lower glacial atmospheric carbon dioxide levels and a change in the deep-water circulation, stratification and carbon storage during the glacial periods that led to more intense and longer-lasting glacial periods (changing from 41 kyr to 100 kyr cycles) and cooler SSTs (Chalk et al., 2017; Clark et al., 2024; Farmer et al., 2019; Kim et al., 2021; Tachikawa et al., 2021; Willeit et al., 2019; McClymont et al., 2013). Early studies (Farmer et al., 2019; McClymont et al., 2013; Pena and Goldstein, 2014) described a major shift in the deep-water circulation during the EMPT, often considered as the first 100 ka cycle and referred to as "the 900 ka event". The new high-resolution timeseries of Hines et al. (2024) revealed, however, no substantial changes in deep-ocean circulation across the EMPT and the authors attributed the observed shift in deep-ocean carbon storage to changes in deep-ocean density stratification, with Southern Ocean conditions playing an important role.

The causes of the long-term patterns of Quaternary climate have been attributed to internal changes in climate response to orbital forcing, as the latter did not change over this time (Clark, 2012; Clark et al., 2006; Hodell and Channell, 2016; Shacketon, 2000). It is believed that the EMPT may have been influenced by ocean-atmosphere system changes, with

declining atmospheric carbon dioxide concentrations and continental ice-sheet growth playing a role (Chalk et al., 2017; Willeit et al., 2019). During the EMPT glacials, lower sea-levels contribute to benthic $\delta^{13}C$ values reaching their lowest levels in 5 million years (Westerhold et al., 2020), which may be caused by exposed continental shelves accelerating the transport of organic carbon into the oceans (Head and Gibbard, 2015). Nowadays, water masses carrying lower $\delta^{13}C$ signals (<0.5 ‰) are formed by convection around Antarctica (Antarctic Intermediate Water, Antarctic Bottom Water/AABW) and spread out into the global ocean basins (Curry and Oppo, 2005; Kroopnick, 1985). Northward and upward expansion of such signals in the Atlantic basin during glacial periods was therefore interpreted to reflect the replacement of North Atlantic Deep Water (NADW) by southern sourced waters and thus a reduced Atlantic Meridional Overturning Circulation (AMOC) (Hodell and Channell, 2016; Raymo et al., 2004; Raymo et al., 1990; Sarnthein et al., 1994). A recent data-model comparison for the last glacial maximum suggests, however, that benthic $\delta^{13}C$ signals in the deep ocean and associated shifts in prevailing water masses should be interpreted as reflecting AMOC depth and not AMOC strength (Muglia and Schmittner, 2021). Throughout the MIS 22-MIS 24 interval, weakening NADW influence is further indicated by neodymium isotope records (Farmer et al., 2019; Kim et al., 2021; Pena and Goldstein, 2014; Tachikawa et al., 2021), although the new record from IODP Site U1479 in the South Atlantic revealed substantial NADW presence during MIS 23 (Hines et al., 2024). A possible explanation for the increase in glacial $\delta^{18}O$ values during the "900 ka event" relates a weak AMOC and low insolation in the Southern Hemisphere during Marine Isotope Stage (MIS) 23 to maximum continental ice volume build-up, which continued to be registered in the subsequent glacials (Elderfield et al., 2012; Pena and Goldstein, 2014). Hines et al. (2024), on the other hand, attribute the signal to increased density stratification between northern (NADW) and southern sourced waters (AABW) and the shoaling of the boundary between those water masses.

Most of the water stored during Quaternary glaciations in the Laurentide, Greenland and European ice sheets was discharged into the North Atlantic Ocean during the last 1.5 Ma, producing short cold events that were often associated with ice-rafted debris (IRD) deposition (Barker et al., 2022; Barker et al., 2021; Hodell and Channell, 2016; Jansen et al., 2000). The effect of ice-cover changes during the EMPT, mainly associated with the "900 ka event", has been reported based on different proxies and in the (sub)polar regions of both hemispheres. In the North Atlantic, Wright and Flower (2002) found extremely cold events from 1000 to 500 ka at ODP Sites 980 (55ºN, 15°W) and 984 (61ºN, 24°W) (Fig. 1), based on the percentage of

polar species *Neogloboquadrina pachyderma* and IRD records, later on corroborated by the 1.7 Ma long records for Site 983 (60°N 24°W) (Barker et al., 2011; Barker et al., 2022). These data, in conjunction with increased reworked nannofossil abundance during the IRD events at Sites 980/981 (Marino et al., 2011), suggest that the Arctic front shifted from a position between those Sites southward and the sea-ice cover expanded greatly during those periods. That scenario is supported by evidence from IODP Site U1314 (56.36°N, 27.88°W), where Hernández-Almeida et al. (2013) observed an abundance of *N. pachyderma* of up to 93 % during the "900 ka event". Between 900 and 675 ka, the same, short-term extreme cold events were registered further south at IODP Site U1385 (Iberian Margin) as cold SST events associated with lower salinities (higher percentages of the C37:4 alkenone) (Rodrigues et al., 2017). All those cold events were associated with a northward and upward penetration of AABW into the mid-latitudinal North Atlantic (Hodell and Channell, 2016; Hodell et al., 2023a; Hernández-Almeida et al., 2015), implicating a reduction in the AMOC depth (Muglia and Schmittner, 2021), especially during the terminal stadial events.

The western Iberian margin is a key area for high-resolution paleoclimatic studies because it is climatologically sensitive to high and low latitude processes. Following the seminal work of Shackleton et al. (2000), it is known that benthic foraminifera $\delta^{18}O$ records from depths greater than 2500 m on the southwestern Portuguese margin reflect an Antarctic climate signal, in particular Antarctic temperature variations, whereas surface water records from the western and southern Portuguese margin mimic the millennial-scale Greenland interstadial/stadial oscillation and thus record northern hemisphere temperature variations. This concept has now been demonstrated for the last 1440 ka with the high-resolution records of IODP Site U1385 (Hodell et al., 2023a).

Furthermore, planktonic foraminifera assemblages are reliable sources for environmental conditions in the western Iberian margin and specific assemblages can identify prevailing oceanographic conditions. At modern conditions, subtropical species, among them *Globigerinoides ruber* white, reflect the influence of the Azores Current (AzC), whereas *Globigerina inflata* and *Neogloboquadrina incompta* represent the Portugal Current and *Globigerinoides bulloides* upwelling events (Salgueiro et al., 2008). Increased abundances of *Turborotalita quinqueloba* and *Neogloboquadrina pachyderma*, on the other hand, can provide insights into past incursions of subpolar waters and southward displacement of the subarctic front (boundary between the subtropical and subpolar gyres) (Eynaud et al., 2009; Girone et al., 2023; Johannessen et al., 1994; Martin-Garcia et al., 2015; Pflaumann et al., 2003; Salgueiro et al., 2010; Singh et al., 2023).

134   Recent studies (Bajo et al., 2020a; Voelker et al., 2015a) confirmed extremely cold SST
135 conditions during stadial climate events of the EMPT also at southern Portuguese margin IODP
136 Site U1387 (Fig. 1). However, detailed information on the surface-water conditions during the
137 "900 ka event" (MIS 24 to MIS 22) and during the lead up to it remains limited. This study,
138 therefore, aims to characterize surface-water conditions at IODP Site U1387 between MIS 28
139 and MIS 18 (1006-750 ka) to better understand the climate dynamics and oceanographic
140 changes that occurred during this critical period. Situated in the northern Gulf of Cadiz, Site
141 U1387 is highly sensitive to changes in the North Atlantic subtropical gyre and to the water
142 mass exchange between the North Atlantic and the Mediterranean Sea. Moreover, the high
143 sedimentation rates ($\geq$20 cm kyr^{-1}) in contourite drifts like the Faro drift, into which Site U1387
144 was drilled, provide exceptional paleoclimate records with high temporal resolution
145 (Hernández-Molina et al., 2016b). For evaluating temperature changes, both in terms of
146 amplitude and timing, and their relationship to the prevailing oceanographic conditions, we
147 produced high-resolution, sub-millennial-scale records of planktonic foraminifera assemblages
148 and SST reconstructions. Using a multi-proxy approach, the SSTs were reconstructed in two
149 ways: 1) converting the planktonic foraminifera assemblages into summer and winter SSTs
150 using a transfer function; and 2) based on the $U^{K'}_{37}$ alkenone index, approximately reflecting
151 annual mean SSTs. Conditions in the subtropical gyre were also inferred from the dominant
152 coiling direction of the planktonic foraminifera species *Globorotalia truncatulinoides* (% GTS)
153 (Billups et al., 2016), although apparent inconsistencies between that proxy data (Billups et al.,
154 2016; 2020) and the gyre strength reconstruction of Wharton et al. (2024) for the last glacial
155 maximum still need to be solved. We compare our data with other available records from the
156 southwestern Iberian margin, as well as sites from the mid-latitudinal North Atlantic. This
157 comparison allows us to contextualize our results within broader regional and global climatic
158 trends, providing insights into the variability and connections between these key areas during
159 the study period. By integrating these records, we aim to improve our understanding of both
160 local and large-scale processes affecting this Northeast Atlantic region.
161
162 **2. Regional Setting**
163   The subtropical gyre nowadays comprises much of the surface and sub-surface waters
164 in the low-to mid-latitudinal North Atlantic, is approximately 1000 km in diameter and
165 distributes heat and moisture to the north (Fig. 1A). The gyre circulation is driven by a
166 combination of trade winds, westerlies and the Coriolis force, whereby the westerlies dominate
167 the circulation in its northern part, especially during the winter. The strength and position of

168   the oceanic currents depend, therefore, on the variability of the atmospheric wind fields. During

169   the winter the latter are characterized by the eastward displacement of cyclonic perturbations

170   (Relvas et al., 2007).

171   Located within the southern mid-latitudinal North Atlantic, the Gulf of Cadiz has a

172   surface-subsurface current system dominated by three branches of the North Atlantic's

173   subtropical gyre circulation: the eastward flowing AzC between 34.3 and 35.7ºN, contributing

174   with heat and salt; the Azores Counter-Current between 37.74 and 39.24ºN and the Canary

175   Current that flows south-westwards (Carracedo Segade et al., 2015). The AzC dominates the

176   Gulf of Cadiz surface waters (0 to 500 m) and partially recirculates along the western Iberian

177   margin through the Iberian Poleward Current that results from the seasonal reversal of the wind

178   regimes (Frouin et al., 1990; Peliz et al., 2005) (Fig. 1B). Also, the Gulf of Cadiz is an important

179   transition zone where the Mediterranean Outflow Water flows at intermediate depth level,

180   adding high salinity and heat to the North Atlantic Circulation (Ambar et al., 1999; Folkard et

181   al., 1997).

182   The Gulf of Cadiz receives contributions from the Portugal Current and the Portugal

183   Coastal Current (Fiuza et al., 1998). The Portugal Current flows equatorward transporting

184   cooler and less saline waters into the region (Carracedo et al., 2014; Peliz et al., 2009). The

185   Portugal Coastal Current exists only during the upwelling season from late May/early June to

186   late September/early October, driven by the northerly winds that transport cold and less saline

187   upwelled water (jet-like) southward (Criado-Aldeanueva et al., 2006; Folkard et al., 1997) (Fig.

188   1B). Near Cape São Vicente, a part of the Portugal Coastal Current jets turns eastward under

189   favorable wind conditions and enters the Gulf of Cadiz flowing along the upper slope toward

190   the Strait of Gibraltar interacting with the upwelling off Cape Santa Maria (Sanchez and

191   Relvas, 2003) and affecting the region of Site U1387.

192   The Gulf of Cadiz SSTs have a seasonal behavior observed by Folkard et al. (1997)

193   through satellite images. Temperatures vary between 22.5 °C (summer) (Fig. 1B) and 16.5 °C

194   (winter) with a mean value of 19.6 °C (Vargas et al., 2003).

195
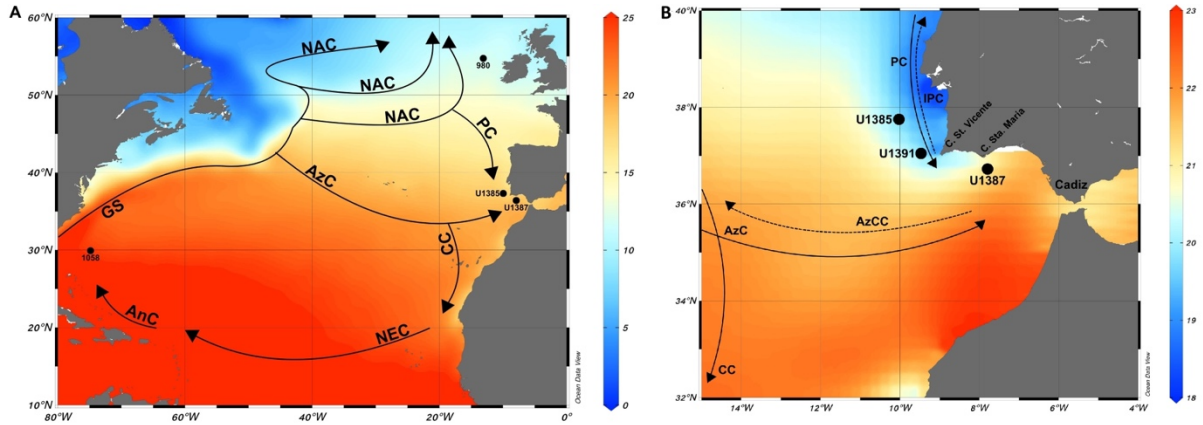
Figure 1: A: North Atlantic Ocean with annual mean SSTs (°C) at 0.25-degree resolution as background (WOA 2023; Reagan et al., 2024). Location of IODP Site U1387 and other available North Atlantic records discussed in the text (IODP Site U1385; ODP Site 980; ODP Site 1058; DSDP Site 607/IODP Site U1313). Black arrows represent the surface circulation: GS – Gulf Stream; NAC – North Atlantic Current; PC – Portugal Current; CC – Canary Current; AzC – Azores Current; NEC – North Equatorial Current; AnC – Antilles Current. B: Close-up of the study area with locations of IODP Site U1387 and SW Iberian Margin IODP Sites U1385 and U1391 with the mean summer (July-September) SSTs (°C) at 0.25-degree resolution as background (WOA 2023; Reagan et al., 2024). Black arrows represent the surface circulation: AzCC – Azores Countercurrent; IPC – Iberian Poleward Current. Currents adapted from Baptista et al. (2021) and references therein. Background maps made with ODV (Schlitzer, 2023).

3. Material and Methods

IODP Site U1387 (36°48.3210'N, 7°43.1321'W) was drilled in December 2011 by the Integrated Ocean Drilling Program (IODP) during Expedition 339 - Mediterranean Outflow into the Faro Drift, northern Gulf of Cadiz, at a water depth of 559 m (Fig. 1) (Expedition 339 Scientists, 2013). The samples were collected at a resolution of 12-13 cm along the revised splice (Voelker et al., 2018), except for the interval of Termination X where the resolution was increased to 6-7 cm for the Bajo et al. (2020a) study. Each sample was freeze-dried, weighed and washed through a 63 µm-mesh sieve, following the procedure established in the Sedimentology and Micropaleontology Laboratory of the Division for Geology and Marine Georesources at the Portuguese Institute for the Sea and Atmosphere (IPMA) (Voelker et al., 2015a). The coarse fraction residue was transferred onto filter paper, dried at 40 °C, and weighed.

3.1 Stable isotope measurements

To establish a stable oxygen isotope record for the chronostratigraphy, 6-12 specimens of the planktonic foraminifera *Globigerinoides bulloides* were collected from the fraction >250 µm of a total of 706 samples. The specimens were sent to the gas isotope ratio mass spectrometry laboratory at MARUM (University Bremen), Germany, where they were analyzed with a Finnigan MAT-251 or MAT-252 mass spectrometer coupled to an automated Kiel I or Kiel III carbonate preparation system, respectively. The mass spectrometers' long-term precision is ±0.07 ‰ for $\delta^{18}O$ based on repeated analyses of internal (Solnhofen limestone) and external (NBS-19) carbonate standards. Some of the isotope results were already published in Bajo et al. (2020a) and are available as Bajo et al. (2020b), although the age model used in the current study differs from those data.

3.2 Planktonic foraminifer assemblage analysis and SST calculations

For the planktonic foraminifera assemblage, a total of 356 samples were analyzed at a sample resolution of 24-25 cm. Each sample was dry sieved to obtain the fractions >250 µm and 150-250 µm. The respective fraction was then split until about 200 specimens remained in the fraction >250 µm and about 100 specimens in the 150-250 µm fraction. Specimens, including identifiable fragments, were counted, and identified in full in each sub-split.

Species identification followed Kučera (2007) and Schiebel and Hemleben (2017). All sinistral coiling *Neogloboquadrina pachyderma* specimens were assigned to *N. pachyderma*, in agreement with the observed morphotypes being similar to those typically found in polar regions (supplementary figure 1). We are using the percentage of *N. pachyderma* to identify cold water incursions of subpolar origin into the Gulf of Cadiz. The assemblage data were converted into relative abundances (percentages) and species grouping into tropical/subtropical, transitional, subpolar/polar habitats according to Kučera (2007). The Azores Current factor was calculated following Salgueiro et al. (2008) and combines the percentages of *Globorotalia inflata*, *Globigerinoides ruber* (white) and *Trilobatus sacculifer*.

To evaluate changes related to the subtropical gyre influence, we used the newly developed proxy of the coiling direction of planktonic foraminifera *G. truncatulinoides,* which is a subsurface dwelling species with five morphotypes. The morphotype type II is exclusive of the Atlantic Ocean and the Mediterranean Sea and is the only type with dextral and sinistral forms (de Vargas et al., 2001; Ujiié et al., 2010). According to Billups et al. (2016), the amount of sinistral coiling direction of this species increases when the subtropical gyre circulation is more intense. Kaiser et al. (2019) related it furthermore to water temperatures at 300 m ($\geq$12

257 °C) and thus the vertical expansion of the warm water sphere of the subtropical gyre. The proxy

258 will be applied for the first time at the eastern margin of the North Atlantic subtropical gyre.

259 Based on the % GTS distribution along the gyre's eastern margin (supplementary figure 2; see

260 also figure 1 in Kaiser et al., 2019) and the western and southern Iberian margin in particular,

261 where higher % GTS values are observed in the regions under AzC and thus warmer,

262 subtropical waters influence (Fig. 1), we are confident that the proxy can be used in our region.

263 For obtaining the % GTS data, we analyzed whenever possible all the individuals in the fraction

264 >250 μm in all the samples where this species was found (332 of 356 samples screened).

265 Intervals with a high sample volume were split before size fractioning. The coiling ratio was

266 obtained using the following formula: % GTS = GTS*100*(GTS+GTD)$^{-1}$ where GTS is the

267 number of sinistral specimens and GTD the number of dextral specimens (Billups et al., 2016;

268 Ducassou et al., 2018). Kaiser et al. (2019) established that % GTS values for the interpretation

269 of paleoceanographic conditions should be based on the counts of ≥20 specimens.

270   Using the relative abundance data in the assemblages, we estimated the SST for winter

271 and summer using the non-distance-weighted (ndw) option of the SIMMAX program

272 (Pflaumann et al., 1996), similar to the Modern Analog Technique (MAT), following Salgueiro

273 et al. (2014). Although Jonkers and Kučera (2019) recently showed that only 10 species

274 dominate the SST calculations, we used the complete set of 27 species utilized by Pflaumann

275 et al. (1996) to be consistent with previous reconstructions in the region (Salgueiro et al., 2014;

276 Salgueiro et al., 2010). SST was calculated using 10 nearest neighbors and the modern analog

277 database compiled by Salgueiro et al. (2014), which combines the North Atlantic database of

278 the MARGO project (Kučera et al., 2005) with additional samples for the Iberian Margin

279 (Salgueiro et al., 2008) and off NW Africa (Salgueiro et al., 2014; Voelker and Salgueiro,

280 2017).

281

282 **3.3 Alkenone SST reconstructions**

283   We also reconstructed SSTs based on the alkenone $U^{K'}_{37}$ index. Alkenones are lipid

284 molecules that are synthesized by coccolithophorid (phytoplankton) and can be extracted from

285 marine sediments using organic solvents. Lipid molecules analyses were done at 24-25 cm

286 resolution (same levels as planktonic foraminifera assemblage data), except for Termination X

287 where the resolution increased to 6-7 cm (Bajo et al., 2020c). Lipid biomarker extraction was

288 done in 338 samples, whereby the SST for the 216 samples between 212.3 and 257.9 c-mcd

289 were already published in Bajo et al. (2020a). Extraction of lipid molecules from freeze-dried

290 sediments followed the procedure established in the DivGM's Biogeochemistry Laboratory

(Rodrigues et al., 2017; Voelker et al., 2015a), which is based on Villanueva et al. (1997). The di-, tri- and tetra-unsaturated alkenones of 37 carbon atoms were analyzed in a Varian Gas chromatograph Model 3800 equipped with a septum programmable injector and a flame ionization detector (GC-FID) with a CPSIL-5 CB column. Hydrogen was used as carrier gas at a flow rate of 2.5 ml/min and n-hexatriacontane as an internal standard to determine concentrations. To estimate SST's, we used the $U^{K'}_{37}$ index based on the di- and tri-unsaturated alkenones ratio and converted it into temperature values using the global core top calibration of Müller et al. (1998), with an analytical uncertainty of ±0.5 °C.

4. Chronostratigraphy and age models

One goal of IODP Expedition 339 was always to use the open ocean records from Site U1385 to establish age models for the contourite sites, which are potentially affected by current sorting and tectonics (Hernández-Molina et al., 2016a) and are too shallow to record a global ocean benthic $\delta^{18}O$ signal. So, for contourite sites like IODP Site U1387 the planned approach was to correlate their *G. bulloides* $\delta^{18}O$ surface water record with the one of Site U1385 and thus to transfer the U1385 age model(s) to the contourite site, under the assumption that those records would be similar in such a narrow region affected by the same surface water masses. That approach was followed in this study using the high-resolution *G. bulloides* $\delta^{18}O$ record (Hodell et al., 2023b) published by Hodell et al. (2023a) as correlation target for the Site U1387 record. One of the age models of Site U1385 was established by tuning its benthic $\delta^{18}O$ record (Hodell et al., 2023a) to the benthic LR04 stack (Lisiecki and Raymo, 2005), whereas an alternative age model applied tuning to the Probstack (Ahn et al., 2017). The age model used throughout this manuscript for Site U1387 uses the LR04 related ages, although, following Hodell et al. (2023b), Probstack based ages (supplementary figure 3) will also be provided with the data uploaded to the PANGAEA world data center. For MIS boundaries we follow Lisiecki and Raymo (2005) and for MIS substage nomenclature Railsback et al. (2015).

5. Results

5.1 *G. bulloides* $\delta^{18}O$ record and chronostratigraphy

Besides the glacial-interglacial cycles of MIS 28 to MIS 18, the *G. bulloides* $\delta^{18}O$ record of Site U1387 reveals millennial-scale stadial-interstadial oscillations, especially following interglacial MIS 25e, MIS 21g, and MIS 19c (Fig. 2A). Notably, an interstadial event occurs within MIS 22 that is also well captured in the Corchia cave $\delta^{18}O$ record (Bajo et al., 2020a). Overall, the record mimics the one of Site U1385 facilitating the tuning and age model

transference (Fig. 2; supplementary fig. 3). The resulting age model for Site U1387 reveals that sedimentation rates were lower during the interglacial intervals dropping to values around 10 cm kyr^{-1} (MIS 19c, MIS 21g), whereas they increased during transitional and glacial periods (Fig. 2C). The same pattern in sedimentation rates is generally observed for the Probstack based age model (supplementary figure 3), although age ranges are shifted towards younger ages in the MIS 21 to MIS 28 interval and there occurs an interval with higher sedimentation rates in early MIS 26. Both the LR04 and Probstack chronologies diverge significantly from the U-Pb dated Corchia Cave speleothem age model of Bajo et al. (2020a, b) in the interval from early MIS 20 to late MIS 25, whereby the speleothem-based ages greatly change the durations of interglacial MIS 23c and MIS 21g and the timing of Termination X (supplementary figure 4).
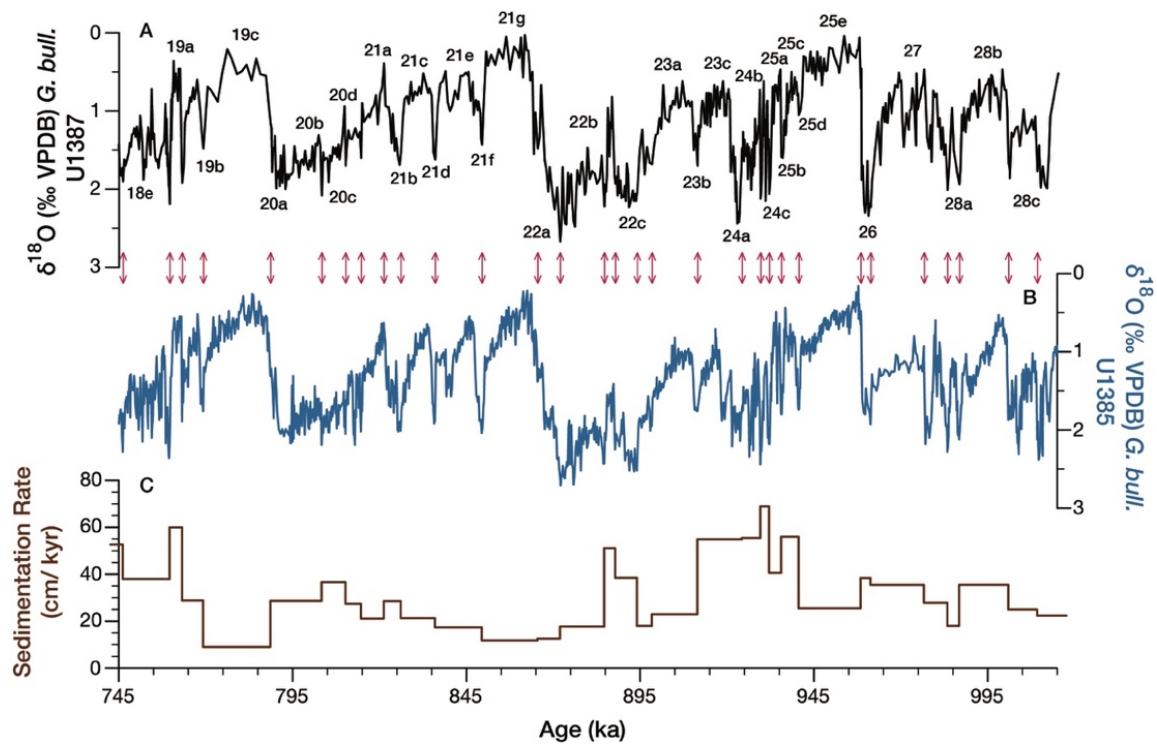
Figure 2: A: δ^{18}O (‰) *G. bulloides* from IODP Site U1387 and Marine Isotopic Stages and Substages. B: δ^{18}O (‰) *G. bulloides* from IODP Site U1385 on its LR04 related age model (Hodell et al., 2023b). Arrows between A and B indicate the tuning points between the two records. C: Sedimentation rates (cm/kyr) for IODP Site U1387.

5.2 Planktonic foraminifera fauna

At Site U1387, we found faunal assemblages composed by a mix of species from polar, subpolar, transitional, subtropical, and tropical provinces (Table 1). In total, 16 species were identified (Table 1; Fig. 3). The diversity of the subtropical fauna appears to be diminished due

346 to the absence of *Globoturborotalita tenella*, *Globoturborotalita rubescens*, and *Globorotalia*

347 *hirsuta*. Although occurring in low percentages, all three species are present in surface and

348 Holocene aged sediments of the southwestern Portuguese margin and in the Gulf of Cadiz (e.g.,

349 Ducassou et al., 2018; Rufino et al., 2022; Salgueiro et al., 2008), and both *Globoturborotalita*

350 *tenella* and *Globoturborotalita rubescens* have been observed in MIS 19 and younger

351 sediments at Site U1385 (Girone et al., 2023; Martin-Garcia et al., 2015).

352

353

354 **Table 1** Species found at IODP Site U1387 and the respective provinces. * indicates species

355 associated with the Azores Current by Storz et al. (2009).

Province	Species
Polar	*Neogloboquadrina pachyderma*
Subpolar	*Neogloboquadrina incompta*
	*Turborotalita quinqueloba**
Transitional	*Globorotalia inflata**
	*Globorotalia scitula**
	*Globigerinita glutinata**
	*Globigerina bulloides**
Subtropical	*Globigerinella calida*
	*Globigerinella siphonifera**
	*Globigerinoides ruber (white)**
	Neogloboquadrina dutertrei
	*Globorotalia truncatulinoides**
	*Globigerina falconensis**
	Orbulina universa
Tropical	*Trilobatus sacculifer**
	Globorotalia crassaformis

356
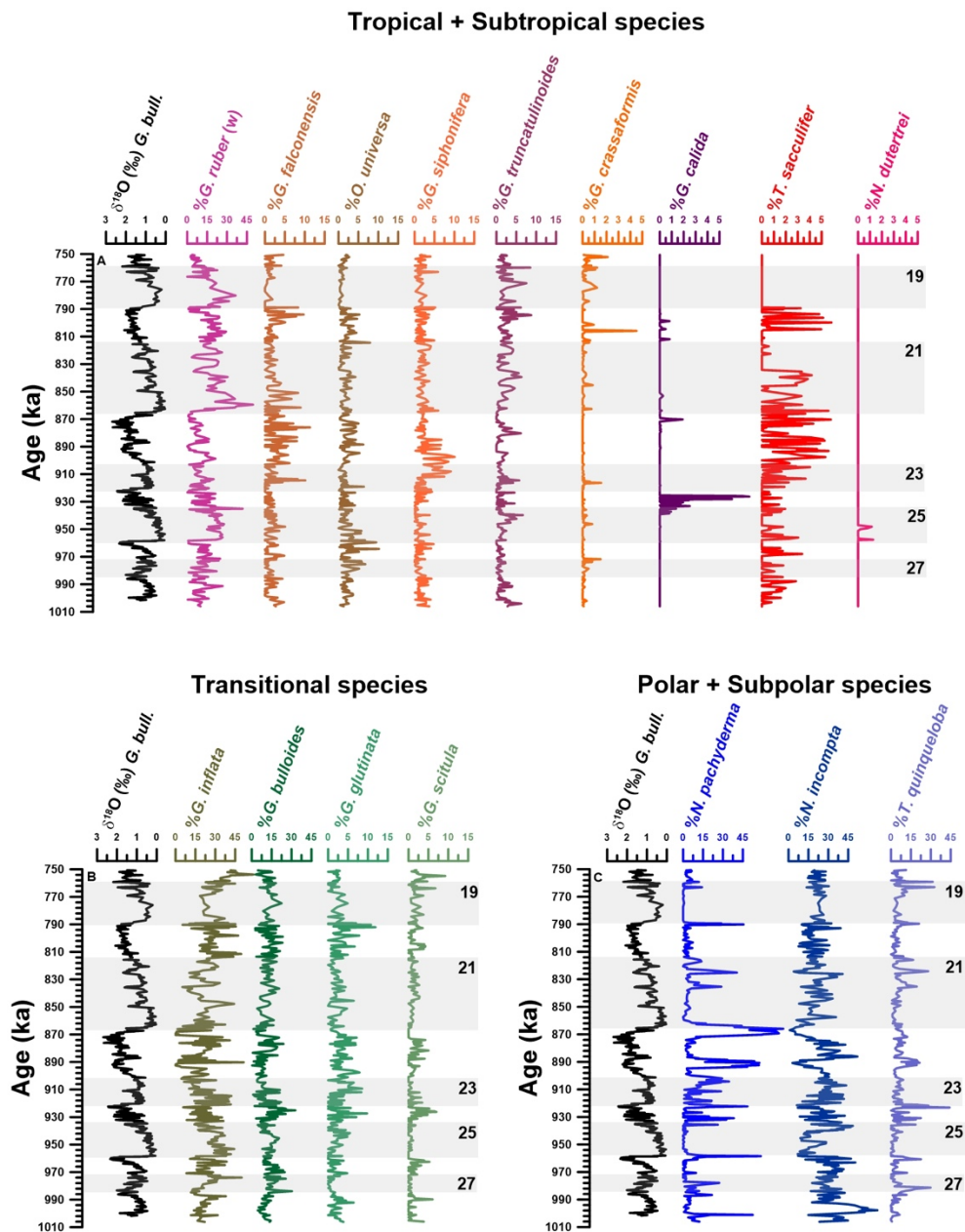
Figure 3: Planktonic foraminifera assemblage from IODP Site U1387. $\delta^{18}O$ *G. bulloides* record (‰ VPDB) (black) provided in all three panels as stratigraphic reference. A: Abundance (%) of tropical species (*Trilobatus sacculifer*; *Globorotalia crassaformis*) and subtropical species (*Globigerinella siphonifera*; *Globigerinoides ruber* (white); *Neogloboquadrina dutertrei*; *Globigerinella calida*; *Orbulina universa*; *Globigerina falconensis*; *Globorotalia truncatulinoides*). B: Abundance (%) of transitional species (*Globorotalia inflata*; *Globorotalia scitula*; *Globigerinita glutinata*; *Globigerina bulloides*). C: Abundance (%) of polar species (*Neogloboquadrina pachyderma*) and subpolar species (*Neogloboquadrina incompta*; *Turborotalita quinqueloba*). Gray bars mark odd-numbered MIS, which include the interglacial periods. Note, differing y-axis scales.

Among all species found, only seven have average abundances greater than 2% over the period studied, i.e. *N. pachyderma, N. incompta, G. inflata, G. ruber* (white)*, T. quinqueloba, G. bulloides,* and *G. glutinata* (Fig. 3). These seven species are among the top 10 ranked by importance for transfer function models (Jonkers and Kučera, 2019). Two additional species from the top 10 list (*T. sacculifer, N. dutertrei*) are present in the samples, but with an abundance of less than 2 %, and one (*G. ruber* pink) is absent. In summary, the results show an alternation of dominance between cold, transitional and warm species through MIS 28 to MIS 18 representing changing conditions in the North Atlantic subtropical gyre.

In general, the transitional group is the more abundant one, with an average abundance of 40.3 %, followed by the polar-subpolar group, 38.8 %, and finally the tropical-subtropical group, 20.2 % (Fig. 4; supplementary table 1). The transitional group is present throughout the studied interval but exhibits behavior like the tropical-subtropical group, i.e. low percentages, during some events when the polar-subpolar group dominates the assemblage.

Seventy-five of the 356 samples screened for % GTS yielded less than 20 specimens (24 with 0 specimens), the cut-off criteria defined by Kaiser et al. (2019), making the % GTS values around 974 ka, 959 ka and 954 ka and in the intervals 923.3-917.8 ka and 893.7-886.8 ka unreliable (Fig. 4B, C). In the earlier part of the record, % GTS increases were less pronounced with three short-term peaks within MIS 28, followed by two peaks during MIS 26 and early MIS 25g. Larger peaks exceeding 80 % GTS occurred between 929.6-927.3 ka, flanking the MIS 22/MIS 21 transition with reliable data centered around 874 ka and 862 ka, and around 823 ka (Fig. 4B).
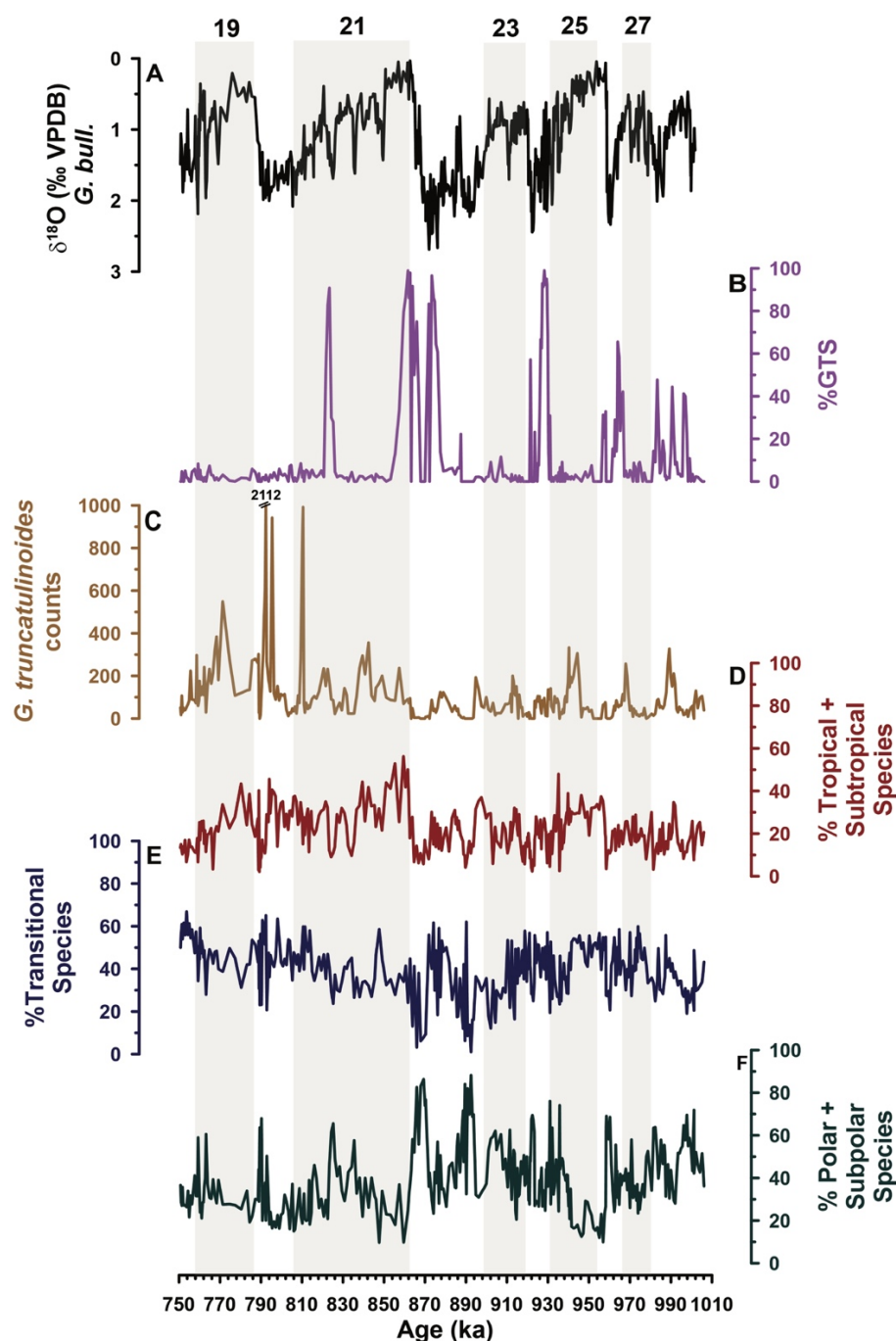
Figure 4: Site U1387 faunal provinces and *Globorotalia truncatulinoides* results. A: δ¹⁸O (‰) *G. bulloides*. B: *G. truncatulinoides* coiling ratio expressed as % of *G. truncatulinoides* (sinistral), showing all the data and thus including not reliable points that are based on fewer than 20 specimens counted (e.g., during the MIS 22/MIS 21 transition). C: Number of *G. truncatulinoides* specimens counted in the fraction >250 μm and used to calculate the coiling ratio in C. D: Abundance (%) summed up for Tropical and Subtropical species. E: Abundance (%) of Transitional species. F: Abundance (%) of Polar and Subpolar species. Grey bars mark the odd-numbered MIS.
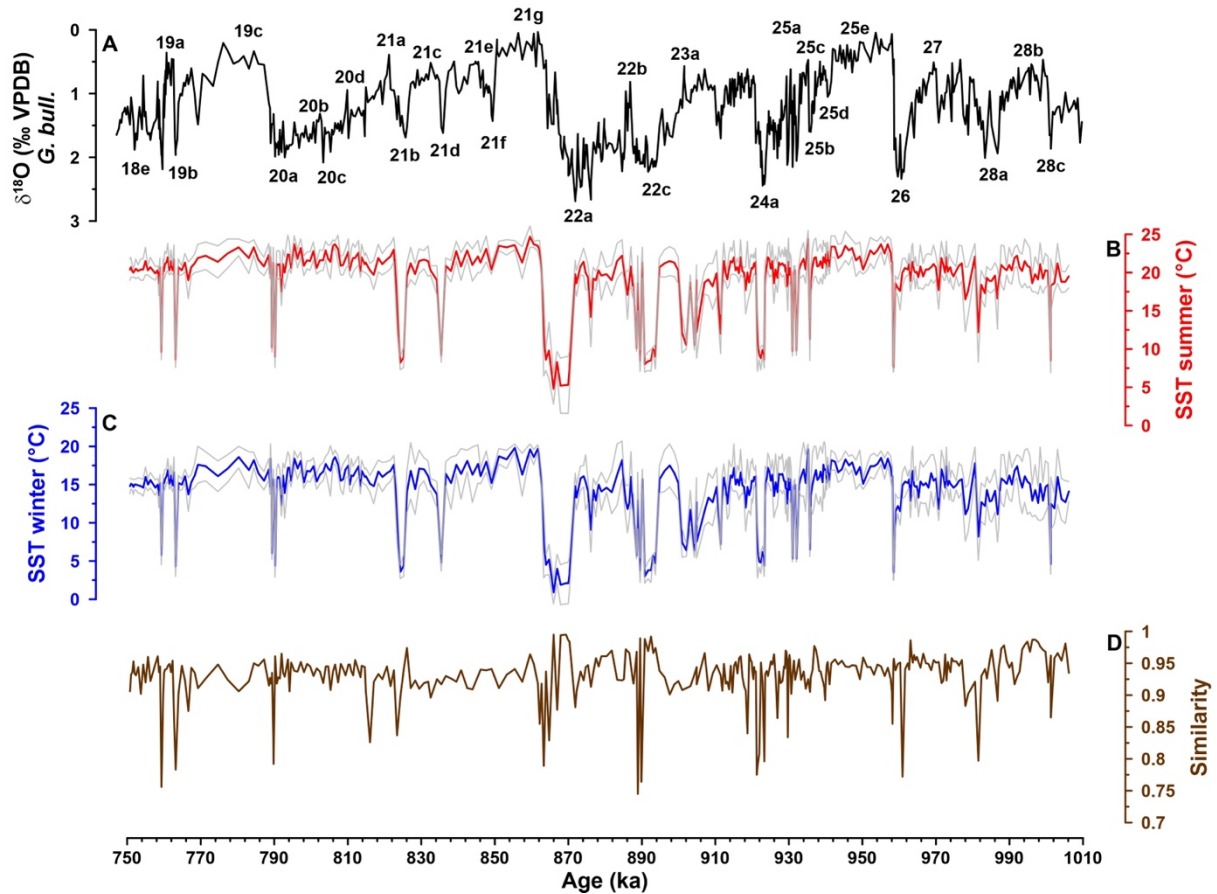
Figure 5: IODP Site U1387 planktonic foraminifera derived SST records A: δ^{18}O *G. bulloides* (‰ VPDB) with numbered Marine Isotopic Stages and Substages. B: Summer SSTs (°C) with standard deviation (1σ). C: Winter SSTs (°C) with standard deviation (1σ). D: Similarity to modern analogs used to calculate the SSTs.

5.3 Sea-Surface Temperatures

The SSTs from IODP Site U1387 estimated with the planktonic foraminifera assemblage (PF-SST) do not reflect a clear pattern for interglacial-glacial cycles from MIS 28 to MIS 18. Although winter SSTs varied between 0.9 to 19.8 °C and summer SSTs between 4.8 to 24.7 °C (Fig. 5), temperatures remained elevated and relative stable during long periods with an average of 14.3 °C for winter and of 19.4 °C for summer, excluding the extremely cold events. Those conditions were interrupted by short, extremely cold events when the percentage of polar and subpolar species increased (Fig. 4F), and winter SSTs dropped below 5 °C (Fig. 5C). Such events occurred during the glacial MIS and during many MIS substages associated with stadial climate conditions (e.g., 25b; 23b; 21d; 21b; 19b). The error (1σ) for the winter SSTs ranges from 0.2 to 4.8 °C and for the summer SSTs from 0.3 to 5.4 °C, with the larger errors associated
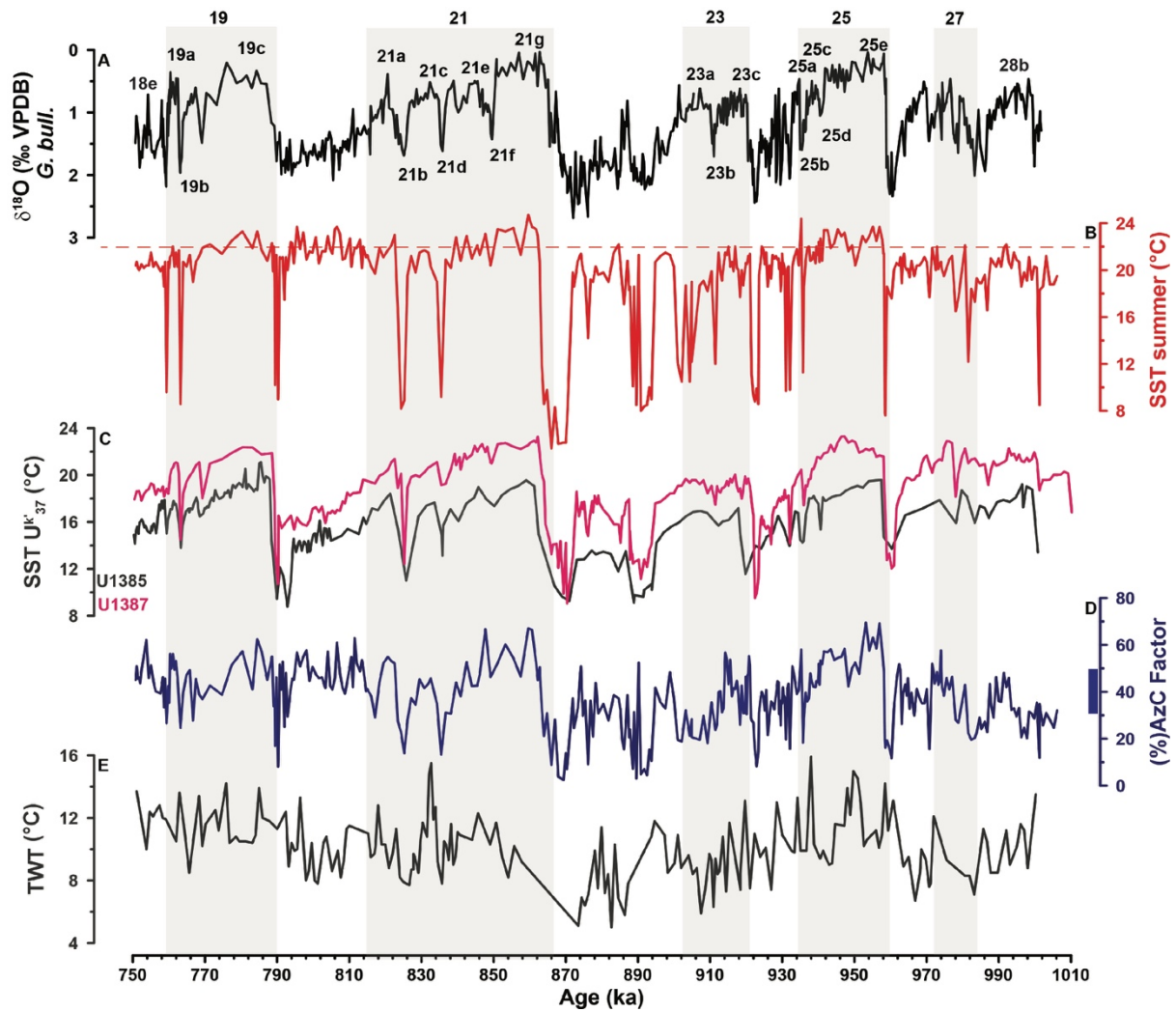
Figure 6: Comparing Site U1387 and Site U1385 temperature records. A: $\delta^{18}O$ *G. bulloides* record of IODP Site U1387 (‰ VPDB) with MIS and substages indicated. B: Planktonic foraminifera Summer SSTs (°C) from Site U1387 with the dashed line marking the late Holocene level of 22°C. C: Alkenone derived SST record of IODP Site U1387 (magenta; Bajo et al., 2020a and this study) in comparison to the Site U1385 record (dark grey; Rodrigues et al., 2017; Rodrigues et al., 2020). D: The Azores Current factor (%) from IODP Site U1387 with the bar next to the scale indicating the modern range in Gulf of Cadiz surface samples (Salgueiro et al., 2008). E: Thermocline water temperature (TWT) at Site U1385 (Bahr et al., 2018; Bahr et al., 2017). Grey bars mark the odd-numbered MIS.

with those samples with lower similarity values (Fig. 5). The similarity between the respective Site U1387 sample and the selected 10 modern analog database samples used to estimate the temperatures is generally above 0.9. Some samples, often associated with extreme cold events, have a lower similarity between 0.9 and 0.75 (Fig. 5D). At these specific lower similarity

433   samples, we observe a small contribution of "warm" species in a dominantly "cold" assemblage

434   leading to a non-analog situation. The species mix and consequently reduced similarity could

435   be linked to bioturbation and/or current transport in those contourite layers (Expedition 339

436   Scientists, 2013) or to the presence of *N. pachyderma* variants with different temperature

437   affinities (see discussion in subchapter 6.3).

438   The alkenone SSTs ($U^{k'}_{37}$-SST) record with annual temperatures ranging from 9.05 to

439   23.3 °C shows a clear glacial/interglacial cycle pattern (Fig. 6). Despite the differences in

440   amplitudes, both techniques registered the extreme cold events contemporaneously,

441   corroborating the interpretation of these results. The coldest period was recorded at the end of

442   MIS 22 between 870.3 and 864.3 ka. During this period, we recorded the highest percentage

443   of *N. pachyderma* (75.5 %) and the lowest temperatures with PF-SST of 4.8 °C for summer

444   and 0.9 °C for winter and $U^{k'}_{37}$-SST of 9.05 °C.

445

446   **6. Discussion**

447   **6.1 Persisting subtropical gyre influence**

448   The strong influence of the AzC in the region is evident through the comparison

449   between the modern planktonic foraminifera assemblage composition (Salgueiro et al., 2008;

450   Rufino et al., 2022) and the reconstructed assemblages from Iberian margin sediments (Girone

451   et al., 2023; Martin-Garcia et al., 2015; Salgueiro et al., 2010; Voelker et al., 2009). During the

452   EMPT, the interglacial and interstadial stages recorded the warmest temperatures, associated

453   with higher percentages of tropical, subtropical and transitional species (Fig. 3; 4D, E).

454   According to Salgueiro et al. (2008), high abundances of *G. ruber* (white), *T. sacculifer* and *G.

455   inflata* at the Iberian margin are indicative of the presence of the AzC's eastern branch (AzC

456   factor; Fig. 6D), whereas Storz et al. (2009) associated a much larger species group with the

457   AzC within the subtropical gyre (Table 1). The relative warm SSTs depicted throughout most

458   of the records, i.e. summer PF-SST within a range of 21 to 24.7 °C and winter PF-SST within

459   15 to 19.8 °C, is associated with the "AzC fauna" that include species from the transitional and

460   subtropical provinces (Salgueiro et al., 2008: Storz et al., 2009); so, we interpret those periods

461   with combined increased abundances of tropical, subtropical, and transitional species and with

462   values for the AzC factor above 30 % (Fig. 6D) as being under AzC and thus subtropical gyre

463   influence.

464   The persistent abundance of *N. incompta* (Fig. 3), slightly above the mean value of 18

465   % observed in the surface sediments (Salgueiro et al., 2008), also points to Portugal Current

466   contributions to the prevailing surface waters as it is a main contributor to the Portugal Current

467 factor (Salgueiro et al., 2008). Whereas higher abundances of *G. bulloides* during the EMPT
468 interglacial periods at western Iberian Margin Site U1391 (Fig. 1B) are interpreted as high
469 productivity upwelling periods (Singh et al., 2015), the same is not observed at Site U1387.
470 Here the percentages of *G. bulloides* generally remain below the local surface sediment mean
471 value of 34 % (Salgueiro et al., 2008) with no distinct glacial/interglacial variations, although
472 percentages increased during glacial MIS 24 and MIS 22 (Fig. 3). We interpret the *G. bulloides*
473 pattern at Site U1387 more as a temperature response, with limited influence of waters
474 upwelled in the major upwelling cell off Cape Saint Vicente (Fig. 1B) and advected towards
475 Site U1387. Nevertheless, the sporadic presence of *Chaetoceros* resting spores (diatoms)
476 within interglacial MIS 25e and MIS 28b (called MIS 27b in cited reference) document some
477 influence of seasonal upwelling at Site U1387 (Ventura et al., 2017). Interestingly, the rare
478 occurrences of planktonic foraminifera *N. dutertrei* in MIS 25e (Fig. 3) coincide with the
479 presence of the large-diameter marine diatom species *Coscinodiscus asteromphalus* (Ventura
480 et al., 2017), which can form large blooms and would thus be an ideal food source for *N.*
481 *dutertrei* (Schiebel and Hemleben, 2017).

482   The $U^{k'}_{37}$-SST data show similar patterns to the PF-SSTs with relatively stable
483 temperatures during interglacial and interstadial substages (Fig. 6), although some intra-
484 interglacial variability is observed (see discussion below). In contrast to the PF-SSTs, the $U^{k'}_{37}$-
485 SSTs reveal a clear cooling trend from the respective interglacial optimum to the subsequent
486 glacial maximum. This different pattern cannot solely be attributed to the $U^{k'}_{37}$-SSTs reflecting
487 annual mean temperatures instead of seasonal ones like the PF-SSTs. During the last glacial
488 maximum, the tropical and subtropical regions cooled (MARGO project members, 2009;
489 Osman et al., 2021; Tierney et al., 2020), so that we should expect climate sensitivity and
490 cooling in those regions also during the EMPT glacial cycles, conforming with the $U^{k'}_{37}$-SST
491 record of Site U1387 and other global records (McClymont et al., 2013; Naafs et al., 2013;
492 Rodrigues et al., 2017). The difference in the reconstructed SST pattern must, therefore, be
493 caused by the planktonic foraminifera fauna itself. While not obvious in the reconstructed PF-
494 SSTs, a decline in the abundance of the AzC species (Fig. 6D), largely driven by declining *G.*
495 *ruber* (white) contributions (Fig. 3), and a contemporary increase in Portugal Current
496 associated species (*G. inflata*, *N. incompta*; Fig. 3) is evident in all those interglacial-glacial
497 cycles, pointing to some cooling also on the zooplankton level. However, the AzC factor fauna
498 (Fig. 6D) and other species linked to subtropical gyre waters (Fig. 4D) retain relative high
499 percentages, so that the transfer function is looking for modern analogs in relative warm waters
500 to estimate the EMPT faunal derived SSTs. Thus, due to the faunas being too similar to modern

subtropical gyre assemblages (Fig. 5D), the estimated PF-SSTs at Site U1387 appear too warm and do not reflect the global cooling, also expected for the North Atlantic subtropical gyre, during the transitions from the glacial inception to the glacial maximum, at least for the glacial cycles covered by this study. The same pattern is also evident for the PF-SSTs obtained for IODP Site U1385 (Martin-Garcia et al., 2015), which also remained warmer than the corresponding $U^{k'}_{37}$-SSTs (Rodrigues et al., 2017).

Site U1387 $U^{k'}_{37}$-SSTs are ~2.5 °C warmer than the $U^{k'}_{37}$-SSTs of IODP Site U1385 on the southwestern Portuguese margin (Fig. 1B), but the overall trends are the same (Fig. 6C). A similar temperature difference between both sites is also visible for the PF-SST reconstructions for MIS 21 to MIS 19, i.e. within the interval the records overlap (Martin-Garcia et al., 2015), although the Site U1385 PF-SSTs were obtained using the artificial neural network method and the original MARGO modern analog database from Kučera et al. (2005). We attribute the temperature gradient to a stronger AzC influence at Site U1387, whereas Site U1385 is more affected by the cooler Portugal Current waters (modern annual mean of 16.1 °C) and by seasonal upwelling (Fig. 1B).

In the Gulf of Cadiz, the summer PF-SSTs and $U^{k'}_{37}$-SSTs reconstructed for the EMPT interglacials were as warm as or slightly warmer than the current interglacial SST (~22 °C; Salgueiro et al., 2014) in the case of the warmer interglacials, i.e. MIS 19c, MIS 21g and MIS 25e, and 1.5 °C cooler during MIS 23c and MIS 27, for which this is only observed in the PF-SSTs (Fig. 6B). However, neither of those interglacial periods experienced surface waters as warm as during early Pleistocene interglacial MIS 47, when $U^{k'}_{37}$-SSTs remained above 24 °C and subtropical planktonic foraminifera abundance mostly above 40 % (Voelker et al., 2022).The warmest EMPT interglacial was MIS 21g, supported by high contributions of the subtropical+tropical fauna of up to 56.3 % *vs*. 45.5 % during MIS 19c and 38 % during MIS 25e (Fig. 4), even though MIS 25e received the higher amount of insolation (Rodrigues et al., 2017). The maximum percentages are comparable to those observed during MIS 47 (generally exceeding 40 % and reaching up to 66.8 %), although periods with such high contributions were much shorter during the EMPT interglacials. Much of the subtropical+tropical fauna abundance is driven by the contribution of *G. ruber* (white) (Fig. 3), which can attribute nearly half of the overall percentage. *G. ruber* (white) added less to the MIS 23c fauna (11 %), but this interglacial had a unique fauna due to the higher influence of subtropical species *G. siphonifera* (2.85 %) (Fig. 3) that persisted into MIS 23a when PF-SSTs became less stable caused by the mixture of planktonic foraminifera provinces (including subpolar and polar species).

Intra-interglacial SST variability is observed during several of the interglacials because a cooling event was recorded in both SST reconstructions during MIS 21g, MIS 23c and MIS 27 leading to a three phased SST evolution, although the timing of the cooling event within the interglacial period varied (Fig. 6). The PF-SSTs documented such a cooling event also for MIS 25e, where it occurred prior to the increase in the $U^{k'}_{37}$-SSTs in the younger phase of the interglacial. As such the MIS 25e $U^{k'}_{37}$-SST pattern mimicked the one of MIS 11c on the Portuguese margin (Rodrigues et al., 2011) and in the mid-latitudinal North Atlantic (Stein et al., 2009), although on a shorter timescale. For both MIS 25e (Ventura et al., 2017) and MIS 11c on the western Portuguese margin (Rodrigues et al., 2011), the early phase of the interglacial is associated with upwelling activity and thus the (temporary) presence of cooler surface waters.

Recently, Barker et al. (2021) proposed to treat MIS 28 as a "missed" interglacial and we therefore include it in our comparison. The summer PF-SST and $U^{k'}_{37}$-SST records of Site U1387 would support such a notion. Specifically, during interstadial MIS 28b, warm PF-SSTs and $U^{k'}_{37}$-SSTs of 19.6 °C and 21.1 °C, respectively, and considerable contributions of the AzC factor fauna suggest to categorize this period as an interglacial (Fig. 6).

Millennial-scale variability in the form of stadial/interstadial oscillations is observed in our records, in accordance with evidence from other North Atlantic sites, evidencing significant modifications in the North Atlantic's thermohaline circulation, the expansion of continental ice sheets and sea ice, and the atmospheric circulation (e.g., Barker et al., 2021; Billups and Scheinwald, 2014; Hernández-Almeida et al., 2015; Hodell and Channell, 2016; Hodell et al., 2023a; Sun et al., 2021; Rodrigues et al., 2017). At Site U1387, one of the most dynamic periods was the interval between MIS 25 and MIS 20, that points to highly variable surface water conditions in the northern subtropical gyre region, in accordance with evidence from DSDP Site 607 and IODP Site U1313 (Marino et al., 2008; Naafs et al., 2013). Here, we focus on the interstadial periods, with the stadials being discussed later in subchapter 6.3. At Site U1387, the interstadials recorded high mean summer PF-SSTs (20.8 °C) similar to the $U^{k'}_{37}$-SSTs (20.0 °C), and a mean winter PF-SSTs of 15.7 °C. The warmest interstadial according to the summer PF-SSTs was MIS 21e with 23.1 °C, whereas the cooler one reached around 19.9 °C (Fig. 5, 6). The interstadials had variable durations with MIS 22b being the longest period with ~16 kyr and MIS 20b the shortest with ~1.5 kyr. Interstadial MIS 22b, occurring during the middle of the glacial MIS 22 and thus within the "900 ka event" period, had a summer PF-SSTs in the general range of 19-21 °C, with the $U^{k'}_{37}$-SSTs being slightly cooler in the 17-18 °C range (Fig. 6). During the interstadials of MIS 23, MIS 22, MIS 21, and MIS 20 noteworthy

569   occurrences of the tropical, surface-dwelling species *T. sacculifer* are observed with 1.9 % on

570   average, but increasing to 2.9 % during MIS 21c (Fig. 3). The periods also registered the

571   greatest abundances of the subtropical species *G. falconensis* (average 2.7 %), increasing to 4.6

572   % during interstadial MIS 20b. Those indicator species, together with the higher AzC factor

573   fauna abundance (Fig. 6D), confirm prevailing subtropical gyre water influence and a strong

574   presence of the AzC at the southern Portuguese margin during the interstadials, in accordance

575   with previous observations on the southwestern margin (Girone et al., 2023; Martin-Garcia et

576   al., 2015; Singh et al., 2015). Those warm surface waters were subducted into the thermocline

577   levels and the subtropical North Atlantic Central Water (Bahr et al., 2018). Bahr et al. (2018)

578   link an intensified AzC, coupled to a strong Mediterranean Outflow Water, to their warmer

579   thermocline water temperatures, which is conforming with our SST and faunal evidence (e.g.,

580   MIS 22b, MIS 21c, MIS 19a) (Fig. 6).

581

582   **6.2 *G. truncatulinoides* evidence for subtropical gyre state**

583   *G. truncatulinoides* is a planktonic foraminifera species that prefers relatively warm,

584   nutrient-rich waters such as at the subtropical gyre margins (Ujiié et al., 2010; Rufino et al.,

585   2022). According to Kaiser et al. (2019) and Feldmeijer et al. (2015), the sinistral variant

586   dominates North Atlantic regions with a deep permanent thermocline, such as the central

587   subtropical gyre. Its presence at mid-latitudinal North Atlantic sites, especially during glacial

588   periods, can indicate the northward flux of subtropical waters and thus the position of the gyre's

589   northern boundary (Kaiser et al., 2019). In contrast, *G. truncatulinoides* (dextral) dominates in

590   the Atlantic's tropical waters and in the cooler subtropical and transitional waters encountered

591   in the NE Atlantic north of 40°N (see supplementary figure 2). High percentages of that variant

592   have been interpreted as reflecting higher contributions of North Equatorial Current and

593   Antilles Current waters (Fig. 1) to the Gulf Stream and thus enhanced westward and northward

594   transport along the western boundary of the subtropical gyre and into its central regions,

595   corresponding with an enhanced gyre circulation overall (Billups et al., 2020).

596   The percentage contributions of *G. truncatulinoides* to the Site U1387 EMPT faunas

597   themselves (Fig. 3) are in the same range as those observed in surface sediments along the

598   western Iberian margin, in the Gulf of Cadiz and the eastern boundary current region off NW

599   Africa (Salgueiro et al., 2008; Rufino et al., 2022). Concerning the coiling direction, the dextral

600   variant dominates during much of the interval, conforming with other North Atlantic sites in

601   gyre boundary locations (Kaiser et al., 2019) (Fig. 7). The foremost characteristics of the %

602   GTS record are, however, increased contributions of the left coiling variant during MIS 28,
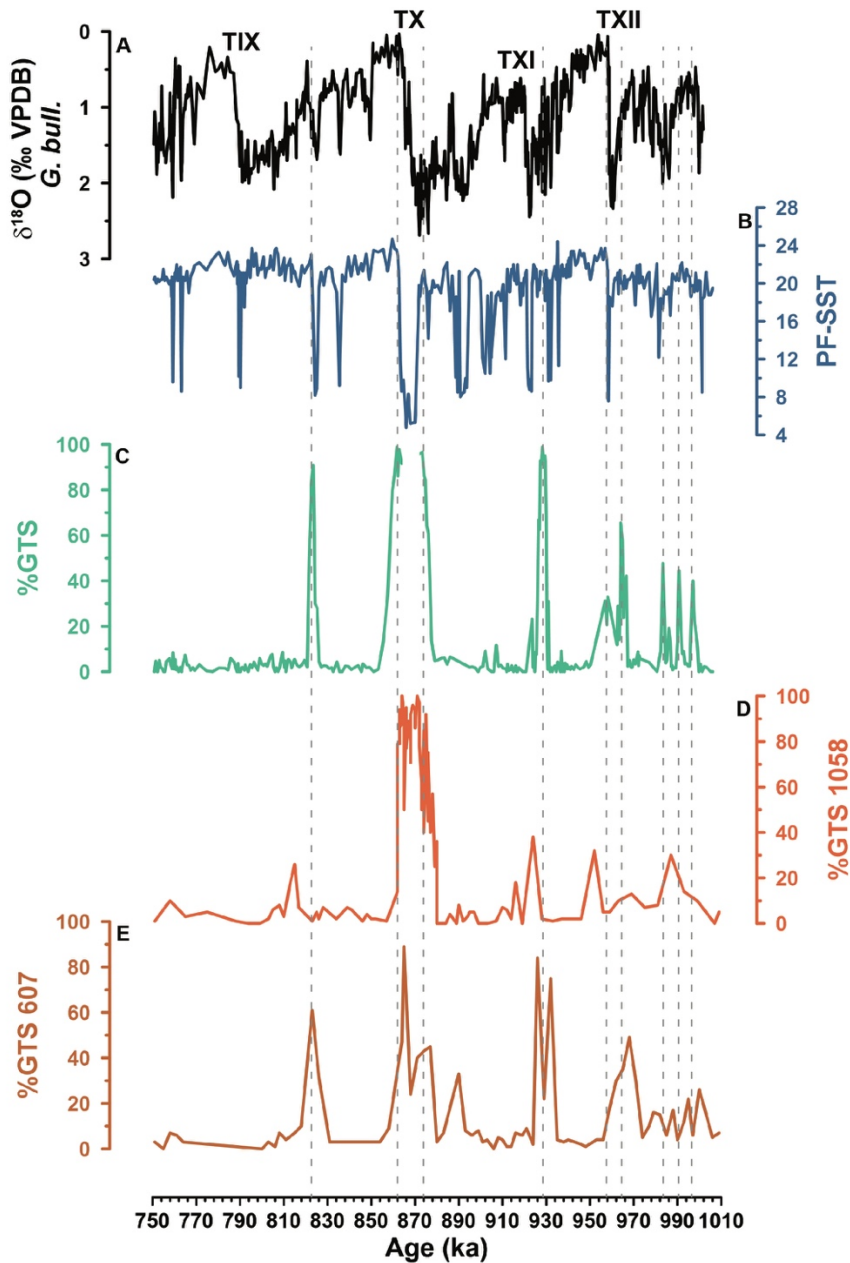
Figure 7: Subtropical gyre intensification episodes**.** A: $\delta^{18}O$ (‰) *G. bulloides* from IODP Site U1387. B: summer PF-SST from IODP Site U1387. C: Coiling ratio (%) of planktonic foraminifera *G. truncatulinoides* (sinistral) from IODP Site U1387 (only showing reliable data points based on counts of ≥20 specimens). D: Coiling ratio (%) of planktonic foraminifera *G. truncatulinoides* (sinistral) from ODP Site 1058 (Kaiser et al., 2019). E: Coiling ratio (%) of planktonic foraminifera *G. truncatulinoides* (sinistral) from DSDP Site 607 (Kaiser et al., 2019). Dashed lines mark peaks of U1387 %GTS maxima. Terminations are indicated by the letter T and the respective Latin numerical.

613 MIS 26, MIS 24, and at the end of stadial MIS 21b and two maxima bracketing the terminal

614 stadial event of Termination X (Fig. 7C). Many of those % GTS peaks have counterparts at

615 northern subtropical gyre Site 607 (Fig. 7E), where those maxima implicate the vicinity of the

616 gyre's northern boundary (Kaiser et al., 2019) and thus a gyre northward expansion not much

617 different from today, in agreement with the relative warm subsurface temperatures

618 reconstructed at the same location (Catunda et al., 2021). The Site U1387 % GTS increases

619 during MIS 28 and MIS 24 and following the terminal stadial event of Termination XII (MIS

620 26/ MIS 25) have no counterparts at Site 607 (Kaiser et al., 2019), at least within the temporal

621 resolution and age model constraints (Fig. 7). With the exception of the event during MIS 24,

622 those % GTS peaks reached mid-range values (30-65 %), similar to those observed in the

623 surface sediments along the southwestern and southern Portuguese margin (supplementary

624 figure 2). So, conditions during those periods were probably comparable to modern conditions

625 with substantial AzC influence and the warm water body of the subtropical North Atlantic

626 Central Water extending down to 250-300 m in the vicinity of Site U1387 (Voelker et al.,

627 2015a, b). With the exception of the early MIS 28 peaks, such a scenario is supported by the

628 AzC related faunal contributions at Site U1387 (Fig. 6D), although, within the age constraints,

629 no related warming events are seen in the Site U1385 thermocline temperature record (Fig.

630 6E).

631   The most prominent feature in the % GTS records of Sites U1387, 607 and 1058 is the

632 period from MIS 22a to MIS 21g when % GTS temporarily reached values between 80 to 100

633 % (Fig. 7). At western boundary/Gulf Stream ODP Site 1058 the feature is one long lasting

634 (~20 kyr) peak, whereas at DSDP Site 607 a double peak is observed. At Site U1387, only the

635 onset and ending of the broader ODP Site 1058 peak are recorded, because during the extreme

636 cold event *G. truncatulinoides* disappeared or nearly disappeared from the faunas indicating

637 the absence of a warm subsurface layer. Based on their Sites 1058 and 607 data, Kaiser et al.

638 (2019) posited that the North Atlantic's subtropical gyre expanded as far north as 41°N (or

639 further) during glacial MIS 22a and that its circulation was more vigorous than during the last

640 glacial maximum (at least based on the % GTS evidence, which, for the last glacial maximum,

641 is not in agreement with the new Wharton et al. (2024) results). This scenario agrees with the

642 warm subsurface temperatures reconstructed at IODP Site U1313 during MIS 22a (Catunda et

643 al., 2021), which were not much cooler than interglacial levels and indicate an expanded layer

644 of subtropical gyre waters. The Site U1387 records (% GTS, AzC factor; Fig. 6D, 7C) now

645 corroborate that the well-developed subtropical gyre extended to the basin's eastern margin,

646 but only during the restricted periods of 877-873 ka and 864-857 ka. During the terminal stadial

647 event of Termination X, the subtropical gyre contracted in the north and east leading to the %
648 GTS minimum at Site 607 and temporary absence of the species at Site U1387, whereas its
649 western boundary remained near the position of Site 1058 (Kaiser et al., 2019). When the
650 subarctic front receded northward after the terminal stadial event of Termination X, the
651 subtropical gyre expanded again into its modern configuration as evidenced by the % GTS
652 maxima at Site 607 and U1387 (Fig. 7). This facilitated subtropical water transport to the north
653 and enabled deep-water convection in the North Atlantic to penetrate once more into depths
654 below 3800 m (Site U1308; Fig. 8G) (Hodell and Channell, 2016; Hodell et al., 2023a; Kaiser
655 et al., 2019), thus the establishment of interglacial conditions.

656   The other two pronounced % GTS peaks at Site U1387, i.e., during MIS 24 and late
657 MIS 21, occurred at the onset of an interstadial that followed a stadial with an extreme cooling
658 event (Fig. 7), when the AzC related fauna was reduced (Fig. 6C) and subtropical gyre water
659 influence therefore diminished (Fig. 7). So, similar to the sequence of events during the onset
660 of MIS 21g, we interpret the % GTS signal as reflecting a well-developed subtropical gyre
661 expanding once more to the Portuguese margin after the subarctic front receded northward.
662 Both % GTS maxima were associated with an increased AzC influence at Site U1387 (Fig.
663 6C), an expanded warm water layer at DSDP Site 607 (% GTS; Fig. 7E)/ IODP Site U1313
664 (subsurface temperature; Catunda et al., 2021) and a deeper AMOC with well-ventilated
665 NADW reaching depths > 3800 m (Fig. 8G; Hodell and Channell, 2016). To account for the
666 high % GTS values, in comparison for example to the smaller % GTS increase at the onset of
667 MIS 25e with an overall similar sequence of climate signals, we postulate that the eastern
668 boundary circulation might have been more vigorous for a short period during the eastward
669 expansion of the gyre.
670
671

672 **6.3 The extreme cold events**
673 Site U1387 recorded several short stadial events (~2 kyr) following the glacial inceptions and
674 as terminal stadial events with winter PF-SSTs dropping to ~5 °C during MIS 24a or even to
675 freezing temperatures of 0 °C during MIS 22a (Fig 5, 8B). The $U^{k'}_{37}$-SSTs during those terminal
676 stadial events also reflect extremely low temperatures, but only reaching 10 °C during MIS 22a
677 and MIS 24a (Fig 6C). The southern position of the subarctic/Arctic front during those stadial
678 periods (Martin-Garcia et al., 2015; Rodrigues et al., 2017), facilitated the presence of the polar
679 species *N. pachyderma,* which reached between 80 % (MIS 22a) and 50 % (MIS 24a) (Fig 8C),
680 as well as a general increase in the number of polar and subpolar species (Fig 8D). The high

percentages of *N. pachyderma* are much higher than those observed during the Heinrich events of the last glacial cycle in the Gulf of Cadiz (< 20 %) and also exceed those observed in general on the southwestern Portuguese margin during the last 400 kyr (<40 %) (Salgueiro et al., 2014; Salgueiro et al., 2010; Singh et al., 2023; Voelker and De Abreu, 2011). They drive the extremely cold SST estimated for the PF-SST, which appears to introduce a "cold bias" for the winter PF-SST that are much colder than the (annual mean) $U^{k'}_{37}$-SSTs (Fig. 6, 8). The *N. pachyderma* morphotypes (supplementary figure 1) are similar to those found today in the subpolar to polar North Atlantic and those observed in contemporary "middle" Pleistocene sediments in the Alboran Sea (western Mediterranean Sea) (Serrano and Guerra-Merchán, 2012). Although *N. pachyderma* adapted to the colder, polar conditions 1100-1000 kyr ago (Huber et al., 2000; Kucera, 2007), thereby establishing the modern polar *N. pachyderma* variant (genotype Ia), a recent review of genetic diversity in planktonic foraminifera from the modern global ocean (Morard et al., 2024) revealed that other *N. pachyderma* genotypes occur only in lower to mid-latitudinal waters of the Atlantic (e.g., Va, VIa), whereby genotype VIa is well established in the mid-latitudinal North Atlantic, especially in the AzC region, and the Mediterranean Sea. Serrano and Guerra-Merchán (2012) postulated that their early Pleistocene *Neogloboquadrina* specimens from the Alboran Sea might include two groups with different temperature affinities, one being the modern polar variant and the other living in warmer waters and/or upwelling conditions. Their observations indicate that the mid-latitudinal North Atlantic genotype VIa or a precursor of it might have already been present in the early Pleistocene. As it is difficult to distinguish between the genotypes based on morphology, it is possible that the Site U1387 EMPT *N. pachyderma* specimens include both the polar and the mid-latitudinal, warmer water affinity variants. Presence of a warmer water variant would agree with the low, but noticeable contemporary presence of various subtropical species and of tropical species *T. sacculifer* in the Site U1387 faunas (Fig. 3, 4D) that hint to some AzC/subtropical gyre influence. This is especially true for MIS 22 when such subtropical water contributions would be consistent with the relative northern expansion of the subtropical gyre (Catunda et al., 2021; Kaiser et al., 2019). Because the modern analog technique used to calculate the PF-SST relies on the percentage contributions of *N. pachyderma* to the total fauna it looks for modern analogs in the Nordic Seas and Labrador Sea and therefore overestimates the cooling, if the % *N. pachyderma* values include relevant contributions of a warm water variant or where that variant dominates. So, for the interpretation of the cold stadial events we give more weight to those events where PF-SSTs and $U^{k'}_{37}$-SSTs show contemporary cooling and caution that some of the extreme cold PF-SSTs might be overestimated.
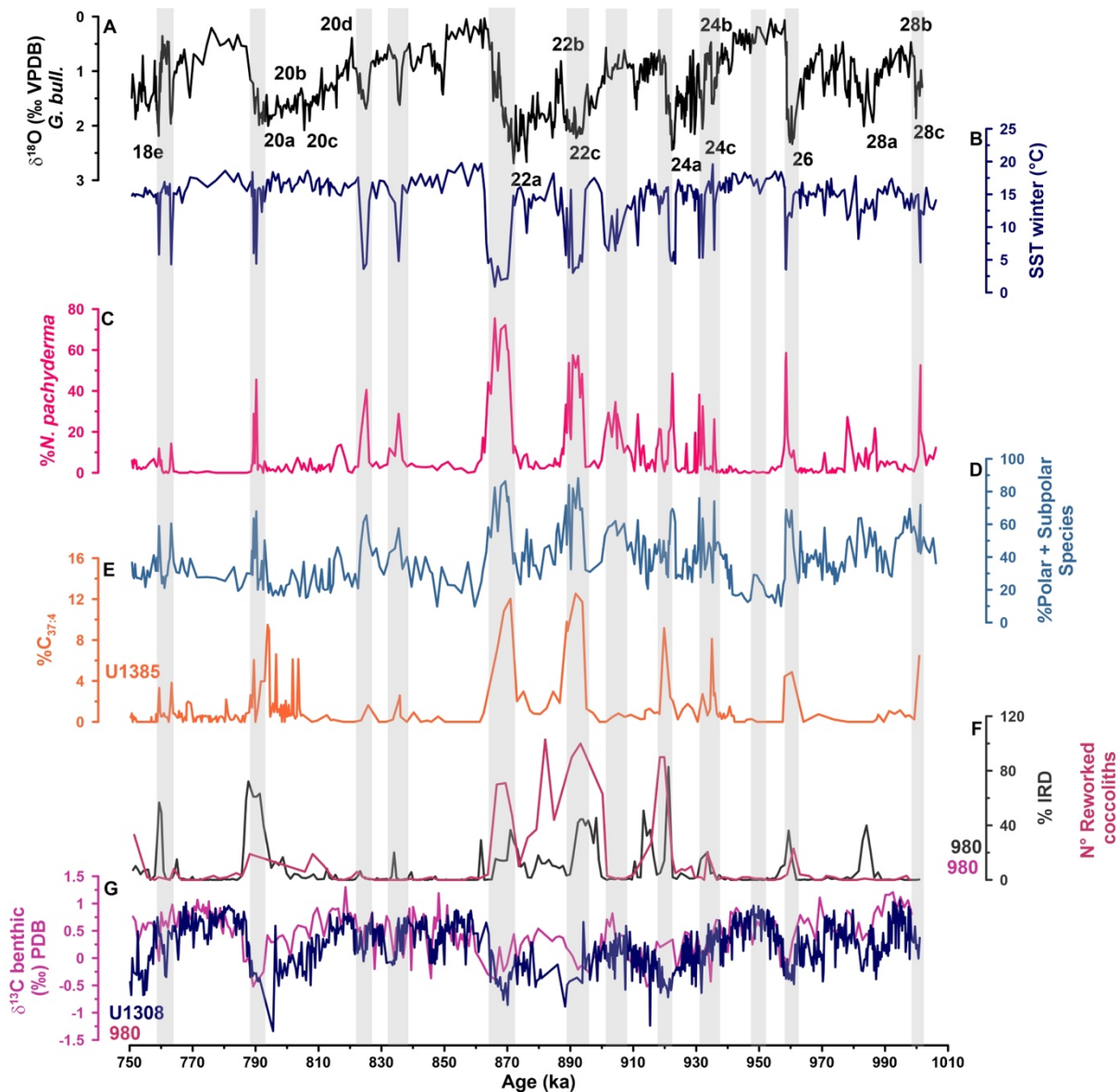
Figure 8: The extreme cold events**.** A: IODP Site U1387 *G. bulloides* δ^{18}O (‰ VPDB) record with MIS and substages. B: Winter PF-SST (°C) from IODP Site U1387. C: Abundance (%) of the planktonic foraminifera *N. pachyderma* from IODP Site U1387. D: Abundance (%) of polar and subpolar species at IODP Site U1387. E: %C[37:4] freshwater indicator from IODP Site U1385 (Rodrigues et al., 2017). F: Number of reworked coccoliths (Marino et al., 2011) and abundance (%) of ice-rafted debris from ODP Site 980 (Wright and Flower, 2002). G: δ^{13}C benthic foraminifera (‰ VPDB) (magenta line) from ODP Site 980 (Wright and Flower, 2002), and δ^{13}C benthic foraminifera (‰) (dark blue line) from IODP Site U1308 (Hodell and Channell, 2016). Gray bars mark cold events.

727   The terminal stadial events (Fig. 8) are all clearly marked in the PF-SSTs and $U^{k'}_{37}$-
728   SSTs record with extreme cooling. The Termination X event (MIS 22a) lasted the longest (6
729   kyr) and was the coldest, registering with lowest SSTs of the whole study interval. In contrast
730   to the southwestern Portuguese margin records from Site U1385 (Girone et al., 2023; Rodrigues
731   et al., 2017), southward incursion of cold surface waters to Site U1387 during Termination IX
732   was much more limited as indicated by the diminished cooling in regard to amplitude and
733   duration. When compared to the others, an atypical terminal stadial event occurred at the end
734   of MIS 28a with low *N. pachyderma* abundances (20 %) and relatively warm PF-SST (10 °C)
735   (Fig. 8). The event presents, however, an assemblage dominated by polar and subpolar species
736   (60 %) and evidence of ice-rafting at ODP Site 980 in the subpolar North Atlantic (Fig. 8F)
737   (Wright and Flower, 2002). All terminal stadial events registered at Site U1387 coincided with
738   ice rafting and melting icebergs in the North Atlantic (Fig. 8E, F) (Hodell and Channell, 2016;
739   Marino et al., 2011; Rodrigues et al., 2017; Wright and Flower, 2002) and a related strong
740   reduction of the AMOC depth as evidenced by the presence of AABW (low benthic $\delta^{13}C$
741   values) in water depths normally occupied by NADW at mid-latitudinal North Atlantic sites
742   from water depths >2500 m (e.g., IODP Sites U1314, U1308, and U1385) (Fig. 8G)
743   (Hernández-Almeida et al., 2015; Hodell and Channell, 2016; Hodell et al., 2023a). The Site
744   U1387 records, therefore, provide further evidence for an extreme contraction of the
745   subtropical gyre in the eastern North Atlantic during those events and indicate that the subarctic
746   front advanced much further south during those events than during the Heinrich events of the
747   last glacial cycle or any terminal stadial events of the last 400 kyr, as already previously
748   suggested by Rodrigues et al. (2017).

749   In addition to the terminal stadial events, there occurred stadial events during MIS 24c,
750   MIS 23b, MIS 21d, MIS 21b, MIS 19b, and MIS 18e with similar environmental characteristics
751   (Fig 8). Although those periods presented lower % *N. pachyderma* between 20 % during MIS
752   18e and 40 % during MIS 24c, the assemblages were dominated by polar and subpolar species
753   (60-80 %) resulting in very cold winter PF-SSTs. The transition to the glacial maximum of
754   MIS 24 was marked by three stadial/interstadial oscillations, with the first two occurring early
755   on and with only 2 kyr separating them. The last stadial was a little cooler (4.9 °C) but was
756   associated with a strong increase in *N. pachyderma* abundance (50 %) and high amounts of
757   IRD (80 %) and reworked coccoliths (90 %) in the subpolar North Atlantic at the ODP Site
758   980 (Marino et al., 2011; Wright and Flower, 2002) (Fig. 8). This evidence, combined with the
759   lower $U^{k'}_{37}$-SST (10 °C) at Site U1387 and the presence of freshwater input at Site U1385

(Rodrigues et al., 2017), indicate a strong southward displacement of the subarctic front also during this event. The cold events in MIS 23b, MIS 21b and MIS 18e were associated with hardly any cooling in the $U^{k'}_{37}$-SSTs (Fig. 6), representing potential cases of "cold bias" in the PF-SSTs.

The transition between MIS 23 and MIS 22 initiated the "900 ka event". Cooler temperatures during MIS 23 could lead to an abrupt increase in Antarctic ice volume and thus lowering of the sea level to 120 m below present (Elderfield et al., 2012). The lower sea level permitted the advance of marine-based ice sheets around the North Atlantic with impacts on ice-rafting and subarctic front movements (Hodell and Channell, 2016). At Site U1387, those background conditions resulted in a cooling event during MIS 23a that is clearly visible in the planktonic foraminifera records, but not the $U^{k'}_{37}$-SST records of either Site U1387 or Site U1385 (Fig. 4, 6, 8). It is, however, contemporary with a short cooling in the subtropical gyre's subsurface waters at Site U1313 (Catunda et al., 2021). The cooling trend initiated with this event culminated in the first, prolonged period of extreme cold conditions during MIS22c at Site U1387 (Fig. 6, 8). In the mid-latitudinal North Atlantic ice-rafting and iceberg melting (Hodell and Channell, 2016; Marino et al., 2011; Wright and Flower, 2002) led to freshening of the surface waters, even as far south as Site U1385 (Fig. 8E) (Rodrigues et al., 2017), and subsequently to a reduction in the AMOC depth as evidenced by the benthic $\delta^{13}C$ records of mid-latitudinal North Atlantic sites from water depths >2100 m (e.g., ODP Site 980/981, IODP Sites U1314, U1308, and U1385) (Fig. 8G) (Hernández-Almeida et al., 2015; Hodell and Channell, 2016; Hodell et al., 2023a; Wright and Flower, 2002). The associated contraction of the subtropical gyre is also reflected in the subsurface waters at Site U1313 cooling by 2 °C to the range of 4 °C (Catunda et al., 2021), a cooling that is not seen during MIS 22a when the subtropical gyre was stronger (Kaiser et al., 2019).

Conclusions

The planktonic foraminifera faunal and SST records of IODP Site U1387 revealed that subtropical gyre waters, especially those related to the AzC, greatly influenced the Gulf of Cadiz during the EMPT interval from MIS 28 to MIS 18, even during the transitions to full glacial conditions following the glacial inceptions. The planktonic foraminifera fauna includes species from all four provinces with the subpolar and polar species dominating during the extreme cold events, in particular the terminal stadial events. The faunal diversity differed slightly from the Holocene, a topic which implications for ecosystem state and restoration

efforts in the region will be explored further in the future. Interglacial periods and several of the interstadials experienced SST as warm or slightly warmer than today and registered persistent AzC influence. The warmest interglacial period was MIS 21g and the coolest, as to be expected from the global climate state, MIS 23. MIS 23 exhibited a particular subtropical planktonic foraminifera fauna, which, in contrast to the other interglacials, included a lesser contribution of *G. ruber* white, but higher ones of *G. falconensis* and *G. siphonifera*. Interestingly, tropical species *T. sacculifer* was present in low percentages throughout MIS 23 and even glacial MIS 22, which included the two periods with the coldest SST of the studied time interval.

Glacial MIS 22a with the terminal stadial event of Termination X stands out as a special time. On the one hand, the highest % *N. pachyderma* and coldest SST during a prolonged period indicate extreme cooling and incursion of subpolar waters into the latitudes of the Gulf of Cadiz. This is only possible if the subarctic front was shifted southward in the eastern North Atlantic. On the other hand, Kaiser et al. (2019) infer the subtropical gyre expanded at least as far north as 41°N, with a vigorous circulation. The % GTS data of Site U1387 agrees in general with such a scenario, although the eastern boundary of the subtropical gyre was in the vicinity of the Gulf of Cadiz only prior to and after the terminal stadial event and a subsurface warm water body was absent during the stadial event itself. As such, the Gulf of Cadiz is once again confirmed as an important confluence region during glacial periods.

Millennial-scale climate variability is clearly recorded as stadial/interstadial SST oscillations during the transition from MIS 25 to MIS 24, whereas during the MIS 21 to MIS 20 transition only MIS 21d and MIS 21b experienced short-term cooling events. Likewise, MIS 19b was associated with a short-term cooling event.

By combining evidence from planktonic foraminifera assemblages with two types of SST reconstructions, we have identified potential biases in our reconstructions. The persistent presence of subtropical gyre and AzC related species in our samples leads to overestimated PF-SSTs following the glacial inceptions and during part of the glacial periods, which becomes obvious in comparison with the $U^{k'}_{37}$-SSTs. On the other hand, the "hidden" presence of a *N. pachyderma* variant with an affinity to warmer AzC current waters, mixed in with the polar variant, probably leads to a cold bias in the PF-SST reconstructions of the extreme cold events. The temporal evolution of *N. pachyderma* and its affinities and potential implications for paleoceanographic reconstructions in the region will be explored in the future, when the Site U1387 planktonic foraminifera faunal records going back to 1500 ka have been completed.

Data availability. The different time series and the planktonic foraminifera faunal data with their respective LR04 and Probstack related age models are archived in the world data center PANGAEA (Felden et al., 2023) and accessible through the reference

Voelker, Antje H L; Mega, Aline; Rodrigues, Teresa (2025): Planktonic foraminifera faunal data and sea-surface temperatures for the Marine Isotope Stage (MIS) 18 to MIS 28 interval of IODP Site 339-U1387, Gulf of Cadiz [dataset bundled publication]. PANGAEA, https://doi.org/10.1594/PANGAEA.974451

Partial records of the *G. bulloides* oxygen isotope and $U^{k'}_{37}$ SST raw data for MIS 21-MIS 26 were already published in Bajo et al. (2020a); note that Bajo et al. (2020b, c) ages listed in PANGAEA differ from the age model(s) used in this manuscript: https://doi.pangaea.de/10.1594/PANGAEA.914401; https://doi.pangaea.de/10.1594/PANGAEA.914400

Supplement. The supplement related to this article is available online at:………..

Author contributions. AHLV initiated and designed the study and secured funding for the biogeochemical and stable isotope analyses. AM produced the planktonic foraminifera faunal data and, together with AHLV, wrote the first draft of the manuscript. ES trained AM in the application of SIMMAX and the interpretation of its results. MP produced the lipid biomarker data under the supervision of TR who also made the final quality control of the results. HK performed the stable isotope analyses at MARUM. All authors, with the exception of MP, who left science in the meantime, read and commented on the draft of the manuscript and approved its final version.

Competing interests. At least one of the (co-)authors is a member of the editorial board of *Climate of the Past*. The authors have no other competing interests to declare.

Acknowledgments. The samples for this study were provided by the Integrated Ocean Drilling Program (2003-2013) and we thank the Bremen Core Repository and its staff for support in sampling the sections. We thank W. Soares, Cremilde Monteiro and the research fellows contracted by the MOWCADYN project for help in preparing the samples in the micropaleontology and sedimentology lab at IPMA. We also thank editor Erin McClymont

860 and the two reviewers for their constructive comments that helped to improve our manuscript

861 and S. Schumacher for the efficient help in archiving our data sets in PANGAEA.

862

863 **Financial support.** The stable isotope and lipid biomarker analyses were made possible

864 through Fundação para a Ciência e a Tecnologia (FCT) funded R&D project MOWCADYN

865 (PTDC/MAR-PRO/3761/2012). Additional financial support from FCT was provided to the

866 Centro de Ciências do Mar do Algarve (CCMAR) through projects: basic funding

867 UIDB/04326/2020 (https://doi.org/10.54499/UIDB/04326/2020); programmatic funding

868 UIDP/04326/2020 (https://doi.org/10.54499/UIDP/04326/2020) and the CIMAR associated

869 laboratory funding LA/P/0101/2020 (https://doi.org/10.54499/LA/P/0101/2020). A. Mega is

870 funded by FCT/CCMAR through PhD fellowship CCMAR01/UIDP/04326/2020. A. Voelker

871 acknowledges her Investigador FCT grant (IF/01500/2014), which provided her salary during

872 the initial phase of the study (2015-2021). The SEM work was made possible through access

873 to the GOLD lab facilities at IPMA funded by the EMSO-PT infrastructure project (POCI-01-

874 0145-FEDER-022157).

875

876 **References**

877 Ahn, S., Khider, D., Lisiecki, L. E., and Lawrence, C. E.: A probabilistic Pliocene–Pleistocene
878 stack of benthic δ^{18}O using a profile hidden Markov model, Dynamics and Statistics of the
879 Climate System, 2, https://doi.org/10.1093/climsys/dzx002, 2017.

880 Ambar, I., Armi, L., Bower, A., and Ferreira, T.: Some aspects of time variability of the
881 Mediterranean Water off south Portugal, Deep-Sea Res Pt I, 46, 1109-1136, 1999.

882 Bahr, A., Kaboth, S., Hodell, D., Zeeden, C., Fiebig, J., and Friedrich, O.: Oceanic heat pulses
883 fueling moisture transport towards continental Europe across the mid-Pleistocene transition,
884 Quaternary Science Reviews, 179, 48-58, https://doi.org/10.1016/j.quascirev.2017.11.009,
885 2018.

886 Bahr, A., Kaboth, S., Hodell, D. A., Zeeden, C., Fiebig, J., and Friedrich, O.: Temperature
887 reconstruction for the Mid-Pleistocene Transition based on deep-dwelling foraminifera of
888 IODP Site339-U1385, https://doi.org/10.1594/PANGAEA.882374, 2017.

889 Bajo, P., Drysdale, R. N., Woodhead, J. D., Hellstrom, J. C., Hodell, D., Ferretti, P., Voelker,
890 A. H. L., Zanchetta, G., Rodrigues, T., Wolff, E., Tyler, J., Frisia, S., Spötl, C., and Fallick,
891 A. E.: Persistent influence of obliquity on ice age terminations since the Middle Pleistocene
892 transition, Science, 367, 1235-1239, https://doi.org/10.1126/science.aaw1114, 2020a.

893 Bajo, P., Drysdale, R. N., Woodhead, J. D., Hellstrom, J. C., Hodell, D. A., Ferretti, P., Voelker,
894 A. H. L., Zanchetta, G., Rodrigues, T., Wolff, E. W., Tyler, J. J., Frisia, S., Spötl, C., and
895 Fallick, A. E.: Oxygen isotope of planktic foraminifera Globigerina bulloides from IODP
896 Site 339-U1387, PANGAEA [dataset], https://doi.org/10.1594/PANGAEA.914401, 2020b.

897 Bajo, P., Drysdale, R. N., Woodhead, J. D., Hellstrom, J. C., Hodell, D. A., Ferretti, P., Voelker,
898 A. H. L., Zanchetta, G., Rodrigues, T., Wolff, E. W., Tyler, J. J., Frisia, S., Spötl, C., and
899 Fallick, A. E.: SST and synchronized ages from IODP Site 339-U1387, PANGAEA
900 [dataset], https://doi.org/10.1594/PANGAEA.914400, 2020c.

Baptista, L., Santos, A. M., Melo, C. S., Rebelo, A. C., Madeira, P., Cordeiro, R., Botelho, A. Z., Hipólito, A., Pombo, J., Voelker, A. H. L., and Ávila, S. P.: Untangling the origin of the newcomer *Phorcus sauciatus* (Mollusca: Gastropoda) in a remote Atlantic archipelago, Marine Biology, 168, 1-16, https://doi.org/10.1007/s00227-020-03808-5, 2021.

Barker, S., Zhang, X., Jonkers, L., Lordsmith, S., Conn, S., and Knorr, G.: Strengthening Atlantic Inflow Across the Mid-Pleistocene Transition, Paleoceanography and Paleoclimatology, 36, e2020PA004200, https://doi.org/10.1029/2020PA004200, 2021.

Barker, S., Knorr, G., Edwards, R. L., Parrenin, F., Putnam, A. E., Skinner, L. C., Wolff, E., and Ziegler, M.: 800,000 Years of Abrupt Climate Variability, Science, 334, 347-351, https://doi.org/10.1126/science.1203580, 2011.

Barker, S., Starr, A., van der Lubbe, J., Doughty, A., Knorr, G., Conn, S., Lordsmith, S., Owen, L., Nederbragt, A., Hemming, S., Hall, I., Levay, L., null, n., Berke, M. A., Brentegani, L., Caley, T., Cartagena-Sierra, A., Charles, C. D., Coenen, J. J., Crespin, J. G., Franzese, A. M., Gruetzner, J., Han, X., Hines, S. K. V., Jimenez Espejo, F. J., Just, J., Koutsodendris, A., Kubota, K., Lathika, N., Norris, R. D., Periera dos Santos, T., Robinson, R., Rolison, J. M., Simon, M. H., Tangunan, D., Yamane, M., and Zhang, H.: Persistent influence of precession on northern ice sheet variability since the early Pleistocene, Science, 376, 961-967, https://doi.org/10.1126/science.abm4033, 2022.

Billups, K. and Scheinwald, A.: Origin of millennial-scale climate signals in the subtropical North Atlantic, Paleoceanography, 29, 612-627, https://doi.org/10.1002/2014PA002641, 2014.

Billups, K., Hudson, C., Kunz, H., and Rew, I.: Exploring *Globorotalia truncatulinoides* coiling ratios as a proxy for subtropical gyre dynamics in the northwestern Atlantic Ocean during late Pleistocene Ice Ages, Paleoceanography, 31, 553-563, https://doi.org/10.1002/2016PA002927, 2016.

Billups, K., Vizcaíno, M., Chiarello, J., and Kaiser, E. A.: Reconstructing Western Boundary Current Stability in the North Atlantic Ocean for the Past 700 Kyr From *Globorotalia truncatulinoides* Coiling Ratios, Paleoceanography and Paleoclimatology, 35, https://doi.org/10.1029/2020PA003958, 2020.

Carracedo, L. I., Gilcoto, M., Mercier, H., and Pérez, F. F.: Seasonal dynamics in the Azores–Gibraltar Strait region: A climatologically-based study, Progress in Oceanography, 122, 116-130, http://dx.doi.org/10.1016/j.pocean.2013.12.005, 2014.

Carracedo Segade, L. I., Gilcoto, M., Mercier, H., and Pérez, F. F.: Quasi-synoptic transport, budgets and water mass transformation in the Azores–Gibraltar Strait region during summer 2009, Progress in Oceanography, 130, 47-64, http://dx.doi.org/10.1016/j.pocean.2014.09.006, 2015.

Catunda, M. C. A., Bahr, A., Kaboth-Bahr, S., Zhang, X., Foukal, N. P., and Friedrich, O.: Subsurface Heat Channel Drove Sea Surface Warming in the High-Latitude North Atlantic During the Mid-Pleistocene Transition, Geophysical Research Letters, 48, https://doi.org/10.1029/2020GL091899, 2021.

Chalk, T. B., Hain, M. P., Foster, G. L., Rohling, E. J., Sexton, P. F., Badger, M. P. S., Cherry, S. G., Hasenfratz, A. P., Haug, G. H., Jaccard, S. L., Martínez-García, A., Pälike, H., Pancost, R. D., and Wilson, P. A.: Causes of ice age intensification across the Mid-Pleistocene Transition, Proceedings of the National Academy of Sciences, 114, 13114-13119, https://doi.org/10.1073/pnas.1702143114, 2017.

Clark, P. U.: Ice Sheets in Transition, Science, 337, 656-658, https://doi.org/10.1126/science.1226335, 2012.

Clark, P. U., Shakun, J. D., Rosenthal, Y., Köhler, P., and Bartlein, P. J.: Global and regional temperature change over the past 4.5 million years, Science, 383, 884-890, https://doi.org/10.1126/science.adi1908, 2024.

Clark, P. U., Archer, D., Pollard, D., Blum, J. D., Rial, J. A., Brovkin, V., Mix, A. C., Pisias, N. G., and Roy, M.: The middle Pleistocene transition: characteristics, mechanisms, and implications for long-term changes in atmospheric pCO_2, Quaternary Science Reviews, 25, 3150-3184, 2006.

Criado-Aldeanueva, F., Garcia-Lafuente, J., Vargas, J. M., Del Rio, J., Vazquez, A., Reul, A., and Sanchez, A.: Distribution and circulation of water masses in the Gulf of Cadiz from in situ observations, Deep Sea Research Part II: Topical Studies in Oceanography, 53, 1144-1160, https://doi.org/10.1016/j.dsr2.2006.04.012, 2006.

Curry, W. B. and Oppo, D. W.: Glacial water mass geometry and the distribution of $\delta^{13}C$ of ΣCO_2 in the western Atlantic Ocean, Paleoceanography, 20, https://doi.org/10.1029/2004PA001021, 2005.

de Vargas, C., Renaud, S., Hilbrecht, H., and Pawlowski, J.: Pleistocene adaptive radiation in *Globorotalia truncatulinoides*: genetic, morphologic, and environmental evidence, Paleobiology, 27, 104-125, https://doi.org/10.1666/0094-8373(2001)027<0104:PARIGT>2.0.CO;2, 2001.

Ducassou, E., Hassan, R., Gonthier, E., Duprat, J., Hanquiez, V., and Mulder, T.: Biostratigraphy of the last 50 kyr in the contourite depositional system of the Gulf of Cádiz, Marine Geology, 395, 285-300, https://doi.org/10.1016/j.margeo.2017.09.014, 2018.

Elderfield, H., Ferretti, P., Greaves, M., Crowhurst, S., McCave, I. N., Hodell, D., and Piotrowski, A. M.: Evolution of Ocean Temperature and Ice Volume Through the Mid-Pleistocene Climate Transition, Science, 337, 704-709, 10.1126/science.1221294, 2012.

Expedition 339 Scientists: Site U1387, in: Proceedings IODP Exp. 339 - Mediterranean Outflow, edited by: Stow, D. A. V., Hernández-Molina, F. J., Alvarez Zarikian, C. A., and the Expedition 339 Scientists, Integrated Ocean Drilling Program Management International, Inc., Tokyo, https://doi.org/10.2204/iodp.proc.339.105.2013, 2013.

Eynaud, F., de Abreu, L., Voelker, A., Schönfeld, J., Salgueiro, E., Turon, J.-L., Penaud, A., Toucanne, S., Naughton, F., Sanchez Goni, M. F., Malaize, B., and Cacho, I.: Position of the Polar Front along the western Iberian margin during key cold episodes of the last 45 ka, Geochem. Geophys. Geosyst., 10, https://doi.org/10.1029/2009GC002398, 2009.

Farmer, J. R., Hönisch, B., Haynes, L. L., Kroon, D., Jung, S., Ford, H. L., Raymo, M. E., Jaume-Seguí, M., Bell, D. B., Goldstein, S. L., Pena, L. D., Yehudai, M., and Kim, J.: Deep Atlantic Ocean carbon storage and the rise of 100,000-year glacial cycles, Nat Geosci, https://doi.org/10.1038/s41561-019-0334-6, 2019.

Felden, J., Möller, L., Schindler, U., Huber, R., Schumacher, S., Koppe, R., Diepenbroek, M., and Glöckner, F.: PANGAEA – Data Publisher for Earth & Environmental Science, Scientific Data, 10, https://doi.org/10.1038/s41597-023-02269-x, 2023.

Feldmeijer, W., Metcalfe, B., Brummer, G. J. A., and Ganssen, G. M.: Reconstructing the depth of the permanent thermocline through the morphology and geochemistry of the deep dwelling planktonic foraminifer *Globorotalia truncatulinoides*, Paleoceanography, 30, 1-22, https://doi.org/10.1002/2014PA002687, 2015.

Fiuza, A. F. G., Hamann, M., Ambar, I., del Rio, G. D., Gonzalez, N., and Cabanas, J. M.: Water masses and their circulation off western Iberia during May 1993, Deep-Sea Res Pt I, 45, 1127-1160, 1998.

Folkard, A. M., Davies, P. A., Fiuza, A. F. G., and Ambar, I.: Remotely sensed sea surface thermal patterns in the Gulf of Cadiz and the Strait of Gibraltar: Variability, correlations, and relationships with the surface wind field, Journal of Geophysical Research, 102, 5669-5683, 1997.

Frouin, R., Fiuza, A. F. G., Ambar, I., and Boyd, T. J.: Observations of a Poleward Surface Current Off the Coasts of Portugal and Spain during Winter, Journal of Geophysical Research, 95, 679-691, 1990.

1001 Girone, A., De Astis, A., Sierro, F. J., Hernández-Almeida, I., Garcia, M. A., Sánchez Goñi,
1002   M. F., Maiorano, P., Marino, M., Trotta, S., and Hodell, D.: Planktonic foraminifera
1003   response to orbital and millennial-scale climate variability at the southern Iberian Margin
1004   (IODP Site U1385) during Marine Isotope Stages 20 and 19, Palaeogeography,
1005   Palaeoclimatology, Palaeoecology, 615, 111450,
1006   https://doi.org/10.1016/j.palaeo.2023.111450, 2023.
1007 Head, M. J. and Gibbard, P. L.: Early–Middle Pleistocene transitions: Linking terrestrial and
1008   marine realms, Quaternary International, 389, 7-46,
1009   https://doi.org/10.1016/j.quaint.2015.09.042, 2015.
1010 Hernández-Almeida, I., Sierro, F. J., Cacho, I., and Flores, J. A.: Subsurface North Atlantic
1011   warming as a trigger of rapid cooling events: evidence from the early Pleistocene (MIS 31–
1012   19), Clim. Past, 11, 687-696, https://doi.org/10.5194/cp-11-687-2015, 2015.
1013 Hernández-Almeida, I., Sierro, F. J., Flores, J.-A., Cacho, I., and Filippelli, G. M.:
1014   Palaeoceanographic changes in the North Atlantic during the Mid-Pleistocene Transition
1015   (MIS 31–19) as inferred from planktonic foraminiferal and calcium carbonate records,
1016   Boreas, 42, 140-159, https://doi.org/10.1111/j.1502-3885.2012.00283.x, 2013.
1017 Hernández-Molina, F. J., Sierro, F. J., Llave, E., Roque, C., Stow, D. A. V., Williams, T., Lofi,
1018   J., Van der Schee, M., Arnáiz, A., Ledesma, S., Rosales, C., Rodríguez-Tovar, F. J., Pardo-
1019   Igúzquiza, E., and Brackenridge, R. E.: Evolution of the gulf of Cadiz margin and southwest
1020   Portugal contourite depositional system: Tectonic, sedimentary and paleoceanographic
1021   implications from IODP expedition 339, Marine Geology, 377, 7-39,
1022   http://dx.doi.org/10.1016/j.margeo.2015.09.013, 2016a.
1023 Hernández-Molina, F. J., Wåhlin, A., Bruno, M., Ercilla, G., Llave, E., Serra, N., Rosón, G.,
1024   Puig, P., Rebesco, M., Van Rooij, D., Roque, D., González-Pola, C., Sánchez, F., Gómez,
1025   M., Preu, B., Schwenk, T., Hanebuth, T. J. J., Sánchez Leal, R. F., García-Lafuente, J.,
1026   Brackenridge, R. E., Juan, C., Stow, D. A. V., and Sánchez-González, J. M.: Oceanographic
1027   processes and morphosedimentary products along the Iberian margins: A new
1028   multidisciplinary approach, Marine Geology, 378, 127-156,
1029   https://doi.org/10.1016/j.margeo.2015.12.008, 2016b.
1030 Hines, S. K. V., Charles, C. D., Starr, A., Goldstein, S. L., Hemming, S. R., Hall, I. R., Lathika,
1031   N., Passacantando, M., and Bolge, L.: Revisiting the mid-Pleistocene transition ocean
1032   circulation crisis, Science, 386, 681-686, doi:10.1126/science.adn4154, 2024.
1033 Hodell, D., Lourens, L., Crowhurst, S., Konijnendijk, T., Tjallingii, R., Jiménez-Espejo, F.,
1034   Skinner, L., Tzedakis, P. C., Abrantes, F., Acton, G. D., Alvarez Zarikian, C. A., Bahr, A.,
1035   Balestra, B., Barranco, E. L., Carrara, G., Ducassou, E., Flood, R. D., Flores, J.-A., Furota,
1036   S., Grimalt, J., Grunert, P., Hernández-Molina, J., Kim, J. K., Krissek, L. A., Kuroda, J., Li,
1037   B., Lofi, J., Margari, V., Martrat, B., Miller, M. D., Nanayama, F., Nishida, N., Richter, C.,
1038   Rodrigues, T., Rodríguez-Tovar, F. J., Roque, A. C. F., Sanchez Goñi, M. F., Sierro
1039   Sánchez, F. J., Singh, A. D., Sloss, C. R., Stow, D. A. V., Takashimizu, Y., Tzanova, A.,
1040   Voelker, A., Xuan, C., and Williams, T.: A reference time scale for Site U1385 (Shackleton
1041   Site) on the SW Iberian Margin, Global and Planetary Change, 133, 49-64,
1042   https://doi.org/10.1016/j.gloplacha.2015.07.002, 2015.
1043 Hodell, D. A. and Channell, J. E. T.: Mode transitions in Northern Hemisphere glaciation: co-
1044   evolution of millennial and orbital variability in Quaternary climate, Clim. Past, 12, 1805-
1045   1828, https://doi.org/10.5194/cp-12-1805-2016, 2016.
1046 Hodell, D. A., Crowhurst, S. J., Lourens, L., Margari, V., Nicolson, J., Rolfe, J. E., Skinner, L.
1047   C., Thomas, N. C., Tzedakis, P. C., Mleneck-Vautravers, M. J., and Wolff, E. W.: A 1.5-
1048   million-year record of orbital and millennial climate variability in the North Atlantic, Clim.
1049   Past, 19, 607-636, https://doi.org/10.5194/cp-19-607-2023, 2023a.

Hodell, D. A., Crowhurst, S. J., Lourens, L. J., Margari, V., Nicolson, J., Rolfe, J. E., Skinner, L. C., Thomas, N. C., Tzedakis, P. C., Mleneck-Vautravers, M. J., and Wolff, E. W.: Oxgyen and carbon isotope data for the planktonic foraminifera Globigerina bulloides at IODP Site 339-U1385, PANGAEA [dataset], https://doi.org/10.1594/PANGAEA.951386, 2023b.

Huber, R., Meggers, H., Baumann, K.-H., Raymo, M. E., and Henrich, R.: Shell size variation of the planktonic foraminifer *Neogloboquadrina pachyderma* sin. in the Norwegian–Greenland Sea during the last 1.3 Myrs: implications for paleoceanographic reconstructions, Palaeogeography, Palaeoclimatology, Palaeoecology, 160, 193-212, https://doi.org/10.1016/S0031-0182(00)00066-3, 2000.

Jansen, E., Fronval, T., Rack, F., and Channell, J. E. T.: Pliocene-Pleistocene ice rafting history and cyclicity in the Nordic Seas during the last 3.5 Myr, Paleoceanography, 15, 709-721, 2000.

Johannessen, T., Jansen, E., Flatøy, A., and Ravelo, A. C.: The relationship between surface water masses, oceanographic fronts and paleoclimatic proxies in surface sediments of the Greenland, Iceland, Norwegian Seas, in: Carbon cycling in the glacial ocean: Constraints on the ocean's role in global change, edited by: Zahn, R., Pedersen, T. F., Kaminski, M. A., and Labeyrie, L., Springer Verlag, Berlin, 61-85, 1994.

Jonkers, L. and Kučera, M.: Sensitivity to species selection indicates the effect of nuisance variables on marine microfossil transfer functions, Clim. Past, 15, 881-891, https://doi.org/10.5194/cp-15-881-2019, 2019.

Kaiser, E. A., Caldwell, A., and Billups, K.: North Atlantic Upper-Ocean Hydrography During the Mid-Pleistocene Transition Evidenced by *Globorotalia truncatulinoides* Coiling Ratios, Paleoceanography and Paleoclimatology, 34, 658-671, https://doi.org/10.1029/2018PA003502, 2019.

Kim, J., Goldstein, S. L., Pena, L. D., Jaume-Seguí, M., Knudson, K. P., Yehudai, M., and Bolge, L.: North Atlantic Deep Water during Pleistocene interglacials and glacials, Quaternary Science Reviews, 269, 107146, https://doi.org/10.1016/j.quascirev.2021.107146, 2021.

Kroopnick, P. M.: The distribution of ^{13}C of $\sum CO_2$ in the world oceans, Deep Sea Research Part A. Oceanographic Research Papers, 32, 57-84, 1985.

Kučera, M.: Planktonic Foraminifera as Tracers of Past Oceanic Environments, in: Proxies in Late Cenozoic Paleoceanography, Developments in Marine Geology, edited by: Hillaire–Marcel, C., and de Vernal, A., 1, Elsevier, 213-262, http://dx.doi.org/10.1016/S1572-5480(07)01011-1, 2007.

Kučera, M., Weinelt, M., Kiefer, T., Pflaumann, U., Hayes, A., Weinelt, M., Chen, M.-T., Mix, A. C., Barrows, T. T., Cortijo, E., Duprat, J., Juggins, S., and Waelbroeck, C.: Reconstruction of sea-surface temperatures from assemblages of planktonic foraminifera: multi-technique approach based on geographically constrained calibration data sets and its application to glacial Atlantic and Pacific Oceans, Quaternary Science Reviews, 24, 951-998, https://doi.org/10.1016/j.quascirev.2004.07.014, 2005.

Lisiecki, L. E. and Raymo, M.: A Pliocene-Pleistocene stack of 57 globally distributed benthic δ^{18}O records, Paleoceanography, 20, https://doi.org/10.1029/2004PA001071, 2005.

MARGO Project Members: Constraints on the magnitude and patterns of ocean cooling at the Last Glacial Maximum, Nature Geosci, 2, 127-132, 10.1038/ngeo411, 2009.

Marino, M., Maiorano, P., and Flower, B. P.: Calcareous nannofossil changes during the Mid-Pleistocene Revolution: Paleoecologic and paleoceanographic evidence from North Atlantic Site 980/981, Palaeogeography, Palaeoclimatology, Palaeoecology, 306, 58-69, https://doi.org/10.1016/j.palaeo.2011.03.028, 2011.

Marino, M., Maiorano, P., and Lirer, F.: Changes in calcareous nannofossil assemblages during the Mid-Pleistocene Revolution, Marine Micropaleontology, 69, 70-90, 2008.

Martin-Garcia, G. M., Alonso-Garcia, M., Sierro, F. J., Hodell, D. A., and Flores, J. A.: Severe cooling episodes at the onset of deglaciations on the Southwestern Iberian margin from MIS 21 to 13 (IODP site U1385), Global and Planetary Change, 135, 159-169, http://dx.doi.org/10.1016/j.gloplacha.2015.11.001, 2015.

McClymont, E. L., Sosdian, S. M., Rosell-Melé, A., and Rosenthal, Y.: Pleistocene sea-surface temperature evolution: Early cooling, delayed glacial intensification, and implications for the mid-Pleistocene climate transition, Earth-Science Reviews, 123, 173-193, http://dx.doi.org/10.1016/j.earscirev.2013.04.006, 2013.

Morard, R., Darling, K. F., Weiner, A. K. M., Hassenrück, C., Vanni, C., Cordier, T., Henry, N., Greco, M., Vollmar, N. M., Milivojevic, T., Rahman, S. N., Siccha, M., Meilland, J., Jonkers, L., Quillévéré, F., Escarguel, G., Douady, C. J., de Garidel-Thoron, T., de Vargas, C., and Kucera, M.: The global genetic diversity of planktonic foraminifera reveals the structure of cryptic speciation in plankton, Biological Reviews, https://doi.org/10.1111/brv.13065, 2024.

Muglia, J. and Schmittner, A.: Carbon isotope constraints on glacial Atlantic meridional overturning: Strength vs depth, Quaternary Science Reviews, 257, 106844, https://doi.org/10.1016/j.quascirev.2021.106844, 2021.

Müller, P. J., Kirst, G., Ruhland, G., von Storch, I., and Rosell-Melé, A.: Calibration of the alkenone paleotemperature index Uk´37 based on core-tops from the eastern South Atlantic and the global ocean (60°N-60°S), Geochim. Cosmochim. Acta, 62, 1757-1772, https://doi.org/10.1016/S0016-7037(98)00097-0, 1998.

Naafs, B. D. A., Hefter, J., and Stein, R.: Millennial-scale ice rafting events and Hudson Strait Heinrich(-like) Events during the late Pliocene and Pleistocene: a review, Quaternary Science Reviews, 80, 1-28, http://dx.doi.org/10.1016/j.quascirev.2013.08.014, 2013.

Osman, M. B., Tierney, J. E., Zhu, J., Tardif, R., Hakim, G. J., King, J., and Poulsen, C. J.: Globally resolved surface temperatures since the Last Glacial Maximum, Nature, 599, 239-244, https://doi.org/10.1038/s41586-021-03984-4, 2021.

Peliz, A., Dubert, J., Santos, A. M. P., Oliveira, P. B., and Le Cann, B.: Winter upper ocean circulation in the Western Iberian Basin—Fronts, Eddies and Poleward Flows: an overview, Deep Sea Research Part I: Oceanographic Research Papers, 52, 621-646, https://doi.org/10.1016/j.dsr.2004.11.005, 2005.

Peliz, A., Marchesiello, P., Santos, A. M. P., Dubert, J., Teles-Machado, A., Marta-Almeida, M., and Le Cann, B.: Surface circulation in the Gulf of Cadiz: 2. Inflow-outflow coupling and the Gulf of Cadiz slope current, Journal of Geophysical Research, 114, https://doi.org/10.1029/2008jc004771, 2009.

Pena, L. D. and Goldstein, S. L.: Thermohaline circulation crisis and impacts during the mid-Pleistocene transition, Science, 345, 318-322, https://doi.org/10.1126/science.1249770, 2014.

Pflaumann, U., Duprat, J., Pujol, C., and Labeyrie, L. D.: SIMMAX: A modern analog technique to deduce Atlantic sea surface temperatures from planktonic foraminifera in deep-sea sediments, Paleoceanography, 11, 15-36, 1996.

Pflaumann, U., Sarnthein, M., Chapman, M., de Abreu, L., Funnell, B., Huels, M., Kiefer, T., Maslin, M., Schulz, H., Swallow, J., van Kreveld, S., Vautravers, M., Vogelsang, E., and Weinelt, M.: Glacial North Atlantic: Sea-surface conditions reconstructed by GLAMAP 2000, Paleoceanography, 18, https://doi.org/10.1029/2002PA000774 2003.

Railsback, L. B., Gibbard, P. L., Head, M. J., Voarintsoa, N. R. G., and Toucanne, S.: An optimized scheme of lettered marine isotope substages for the last 1.0 million years, and the climatostratigraphic nature of isotope stages and substages, Quaternary Science Reviews, 111, 94-106, http://dx.doi.org/10.1016/j.quascirev.2015.01.012, 2015.

Raymo, M. E., Ruddiman, W. F., Shackleton, N. J., and Oppo, D. W.: Evolution of Atlantic-Pacific δ13C gradients over the last 2.5 m.y., Earth and Planetary Science Letters, 97, 353-368, 1990.

Raymo, M. E., Oppo, D. W., Flower, B. P., Hodell, D. A., McManus, J. F., Venz, K. A., Kleiven, K. F., and McIntyre, K.: Stability of North Atlantic water masses in face of pronounced climate variability during the Pleistocene, Paleoceanography, 19, https://doi.org/10.1029/2003PA000921, 2004.

Reagan, J. R., Boyer, T. P., García, H. E., Locarnini, R. A., Baranova, O. K., Bouchard, C., Cross, S. L., Mishonov, A. V., Paver, C. R., Seidov, D., Wang, Z., and Dukhovskoy, D.: World Ocean Atlas 2023, NCEI Accession 0270533, NOAA National Centers for Environmental Information [dataset], 2024.

Relvas, P., Barton, E. D., Dubert, J., Oliveira, P. B., Peliz, A., da Silva, J. C. B., and Santos, A. M. P.: Physical oceanography of the western Iberia ecosystem: Latest views and challenges, Progress in Oceanography, 74, 149-173, 10.1016/j.pocean.2007.04.021, 2007.

Rodrigues, T., Voelker, A. H. L., Grimalt, J. O., Abrantes, F., and Naughton, F.: Iberian Margin sea surface temperature during MIS 15 to 9 (580-300 ka): Glacial suborbital variability versus interglacial stability, Paleoceanography, 26, https://doi.org/10.1029/2010PA001927, 2011.

Rodrigues, T., Alonso-García, M., Hodell, D. A., Rufino, M., Naughton, F., Grimalt, J. O., Voelker, A. H. L., and Abrantes, F.: A 1-Ma record of sea surface temperature and extreme cooling events in the North Atlantic: A perspective from the Iberian Margin, Quaternary Science Reviews, 172, 118-130, https://doi.org/10.1016/j.quascirev.2017.07.004, 2017.

Rodrigues, T., Alonso-Garcia, M., Hodell, D. A., Rufino, M. M., Naughton, F., Grimalt, J. O., Voelker, A. H. L., and Abrantes, F. F.: A 1 Ma record of Sea Surface Temperature and extreme cooling events in the North Atlantic: A perspective from the Iberian Margin, PANGAEA [dataset], https://doi.org/10.1594/PANGAEA.921577, 2020.

Rufino, M. M., Salgueiro, E., Voelker, A. A. H. L., Polito, P. S., Cermeño, P. A., and Abrantes, F.: Ocean kinetic energy and photosynthetic biomass are important drivers of planktonic foraminifera diversity in the Atlantic Ocean, Frontiers in Marine Science, 9, https://doi.org/10.3389/fmars.2022.887346, 2022.

Salgueiro, E., Voelker, A. H. L., de Abreu, L., Abrantes, F., Meggers, H., and Wefer, G.: Temperature and productivity changes off the western Iberian margin during the last 150 ky, Quaternary Science Reviews, 29, 680-695, https://doi.org/10.1016/j.quascirev.2009.11.013, 2010.

Salgueiro, E., Naughton, F., Voelker, A. H. L., de Abreu, L., Alberto, A., Rossignol, L., Duprat, J., Magalhães, V. H., Vaqueiro, S., Turon, J. L., and Abrantes, F.: Past circulation along the western Iberian margin: a time slice vision from the Last Glacial to the Holocene, Quaternary Science Reviews, 106, 316-329, https://doi.org/10.1016/j.quascirev.2014.09.001, 2014.

Salgueiro, E., Voelker, A., Abrantes, F., Meggers, H., Pflaumann, U., Loncaric, N., Gonzalez-Alvarez, R., Oliveira, P., Bartels-Jonsdottir, H. B., Moreno, J., and Wefer, G.: Planktonic foraminifera from modern sediments reflect upwelling patterns off Iberia: Insights from a regional transfer function, Marine Micropaleontology, 66, 135-164, https://doi.org/10.1016/j.marmicro.2007.09.003, 2008.

Sanchez, R. F. and Relvas, P.: Spring-summer climatological circulation in the upper layer in the region of Cape St. Vincent, Southwest Portugal, ICES Journal of Marine Science, 60, 1232-1250, https://doi.org/10.1016/S1054-3139(03)00137-1, 2003.

Sarnthein, M., Winn, K., Jung, S., Duplessy, J., Labeyrie, L., Erlenkeuser, H., and Ganssen, G.: Changes in east Atlantic deepwater circulation over the last 30,000 years: Eight time slices reconstructions, Paleoceanography, 9, 209-267, 1994.

Schiebel, R. and Hemleben, C.: Planktic Foraminifers in the Modern Ocean, Springer Verlag, Berlin Heidelberg, 358 pp., https://doi.org/10.1007/978-3-662-50297-6, 2017.

Schlitzer, R.: Ocean Data View, odv.awi.de [code], 2023.

Serrano, F. and Guerra-Merchán, A.: Sea-surface temperature for left-coiling *Neogloboquadrina* populations inhabiting the westernmost Mediterranean in the middle Pleistocene and the Pleistocene-Pliocene transition, Geobios, 45, 231-240, https://doi.org/10.1016/j.geobios.2011.04.003, 2012.

Shacketon, N. J.: The 100,000-Year Ice-Age Cycle Identified and Found to Lag Temperature, Carbon Dioxide, and Orbital Eccentricity, Science, 289, 1897-1902, 2000.

Shackleton, N. J., Hall, M. A., and Vincent, E.: Phase relationships between millennial-scale events 64,000-24,000 years ago, Paleoceanography, 15, 565-569, 2000.

Singh, A. D., Verma, K., Jaiswal, S., Alonso-Garcia, M., Li, B., and Abrantes, F.: Planktic foraminiferal responses to orbital scale oceanographic changes off the western Iberian margin over the last 900 kyr: Results from IODP site U1391, Global and Planetary Change, 135, 47-56, http://dx.doi.org/10.1016/j.gloplacha.2015.10.002, 2015.

Singh, H., Singh, A. D., Tripathi, R., Singh, P., Verma, K., Voelker, A. H. L., and Hodell, D. A.: Centennial-millennial scale ocean-climate variability in the northeastern Atlantic across the last three terminations, Global and Planetary Change, 223, 104100, https://doi.org/10.1016/j.gloplacha.2023.104100, 2023.

Stein, R., Hefter, J., Gruetzner, J., Voelker, A., and Naafs, B. D. A.: Variability of surface-water characteristics and Heinrich-like Events in the Pleistocene mid-latitude North Atlantic Ocean: Biomarker and XRD records from IODP Site U1313 (MIS 16 – 9), Paleoceanography, 24, https://doi.org/10.1029/2008PA001639, 2009.

Storz, D., Schulz, H., Waniek, J. J., Schulz-Bull, D. E., and Kucera, M.: Seasonal and interannual variability of the planktic foraminiferal flux in the vicinity of the Azores Current, Deep Sea Research Part I: Oceanographic Research Papers, 56, 107-124, 2009.

Sun, Y., McManus, J. F., Clemens, S. C., Zhang, X., Vogel, H., Hodell, D. A., Guo, F., Wang, T., Liu, X., and An, Z.: Persistent orbital influence on millennial climate variability through the Pleistocene, Nat Geosci, 14, 812-818, https://doi.org/10.1038/s41561-021-00794-1, 2021.

Tachikawa, K., Rapuc, W., Vidal, L., Dubois-Dauphin, Q., Westerhold, T., Guihou, A., Bickert, T., Pérez-Asensio, J. N., Deschamps, P., and Skonieczny, C.: Eastern Atlantic deep-water circulation and carbon storage inferred from neodymium and carbon isotopic compositions over the past 1.1 million years, Quaternary Science Reviews, 252, 106752, https://doi.org/10.1016/j.quascirev.2020.106752, 2021.

Tierney, J. E., Zhu, J., King, J., Malevich, S. B., Hakim, G. J., and Poulsen, C. J.: Glacial cooling and climate sensitivity revisited, Nature, 584, 569-573, https://doi.org/10.1038/s41586-020-2617-x, 2020.

Ujiié, Y., de Garidel-Thoron, T., Watanabe, S., Wiebe, P., and de Vargas, C.: Coiling dimorphism within a genetic type of the planktonic foraminifer Globorotalia truncatulinoides, Marine Micropaleontology, 77, 145-153, http://dx.doi.org/10.1016/j.marmicro.2010.09.001, 2010.

Vargas, J. M., Garcia-Lafuente, J., Delgado, J., and Criado, F.: Seasonal and wind-induced variability of Sea Surface Temperature patterns in the Gulf of Cadiz, Journal of Marine Systems, 38, 205-219, 2003.

Ventura, C., Abrantes, F., Loureiro, I., and Voelker, A. H. L.: Data report: diatom and silicoflagellate records of marine isotope Stages 25–27 at IODP Site U1387, Faro Drift, https://doi.org/10.2204/iodp.proc.339.202.2017, 2017.

Villanueva, J., Grimalt, J. O., Cortijo, E., Vidal, L., and Labeyrie, L.: A biomarker approach to the organic matter deposited in the North Atlantic during the last climatic cycle, Geochim. Cosmochim. Acta, 61, 4633-4646, 1997.

Voelker, A. H. L. and de Abreu, L.: A Review of Abrupt Climate Change Events in the Northeastern Atlantic Ocean (Iberian Margin): Latitudinal, Longitudinal and Vertical Gradients, in: Abrupt Climate Change: Mechanisms, Patterns, and Impacts, edited by: Rashid, H., Polyak, L., and Mosley-Thompson, E., Geophysical Monograph Series, 193, AGU, Washington D.C., 15-37, https://doi.org/10.1029/2010GM001021, 2011.

Voelker, A. H. L. and Salgueiro, E.: Planktonic foraminifera assemblages in NE Atlantic and Alboran Sea surface sediments, PANGAEA [dataset], https://doi.org/10.1594/PANGAEA.878069, 2017.

Voelker, A. H. L., de Abreu, L., Schönfeld, J., Erlenkeuser, H., and Abrantes, F.: Hydrographic Conditions Along the Western Iberian Margin During Marine Isotope Stage 2, Geochem. Geophys. Geosyst., 10, https://doi.org/10.1029/2009GC002605, 2009.

Voelker, A. H. L., Rodrigues, T., Trotta, S., Marino, M., and Kuhnert, H.: A Southern Portuguese Margin Perspective of Marine Isotope Stage 47 – An Interglacial in the 41 kyr World, Atmosphere, 13, 1-25, https://doi.org/10.3390/atmos13091378, 2022.

Voelker, A. H. L., Jimenez-Espejo, F. J., Bahr, A., Rebotim, A., Cavaleiro, C., Salgueiro, E., and Röhl, U.: Data report: IODP Site U1387: the revised splice between Sections U1387B-18X-3 and U1387C-8R-3 (>171.6 mcd), https://doi.org/10.2204/iodp.proc.339.204.2018, 2018.

Voelker, A. H. L., Salgueiro, E., Rodrigues, T., Jimenez-Espejo, F. J., Bahr, A., Alberto, A., Loureiro, I., Padilha, M., Rebotim, A., and Röhl, U.: Mediterranean Outflow and surface water variability off southern Portugal during the early Pleistocene: A snapshot at Marine Isotope Stages 29 to 34 (1020–1135 ka), Global and Planetary Change, 133, 223-237, https://doi.org/10.1016/j.gloplacha.2015.08.015, 2015a.

Voelker, A. H. L., Colman, A., Olack, G., Waniek, J. J., and Hodell, D.: Oxygen and hydrogen isotope signatures of Northeast Atlantic water masses, Deep Sea Research Part II: Topical Studies in Oceanography, 116, 89-106, 10.1016/j.dsr2.2014.11.006, 2015b.

Westerhold, T., Marwan, N., Drury, A. J., Liebrand, D., Agnini, C., Anagnostou, E., Barnet, J. S. K., Bohaty, S. M., De Vleeschouwer, D., Florindo, F., Frederichs, T., Hodell, D. A., Holbourn, A. E., Kroon, D., Lauretano, V., Littler, K., Lourens, L. J., Lyle, M., Pälike, H., Röhl, U., Tian, J., Wilkens, R. H., Wilson, P. A., and Zachos, J. C.: An astronomically dated record of Earth's climate and its predictability over the last 66 million years, Science, 369, 1383-1387, https://doi.org/10.1126/science.aba6853, 2020.

Wharton, J. H., Renoult, M., Gebbie, G., Keigwin, L. D., Marchitto, T. M., Maslin, M. A., Oppo, D. W., and Thornalley, D. J. R.: Deeper and stronger North Atlantic Gyre during the Last Glacial Maximum, Nature, 632, 95-100, https://doi.org/10.1038/s41586-024-07655-y, 2024.

Willeit, M., Ganopolski, A., Calov, R., and Brovkin, V.: Mid-Pleistocene transition in glacial cycles explained by declining CO_2 and regolith removal, Science Advances, 5, eaav7337, https://doi.org/10.1126/sciadv.aav7337, 2019.

Wright, A. K. and Flower, B. P.: Surface and deep ocean circulation in the subpolar North Atlantic during the mid-Pleistocene revolution, Paleoceanography, 17, https://doi.org/10.1029/2002PA000782, 2002.